

A deep search for the host galaxies of GRBs with no detected optical afterglow[★]

A. Rossi¹, S. Klose¹, P. Ferrero^{2,3}, J. Greiner⁴, L. A. Arnold⁵, E. Gonsalves⁶, D. H. Hartmann⁷, A. C. Updike⁸,
D. A. Kann¹, T. Krühler^{4,9,10}, E. Palazzi¹¹, S. Savaglio⁴, S. Schulze¹², P. M. J. Afonso¹³, L. Amati¹¹,
A. J. Castro-Tirado¹⁴, C. Clemens⁴, R. Filgas⁴, J. Gorosabel¹⁴, L. K. Hunt¹⁵, A. Küpcü Yoldaş¹⁶, N. Masetti¹¹,
M. Nardini¹⁷, A. Nicuesa Guelbenzu¹, F. Olivares E.⁴, E. Pian^{11,18,19}, A. Rau⁴, P. Schady⁴, S. Schmidl¹, A. Yoldaş¹⁶,
and A. de Ugarte Postigo^{10,14}

(Affiliations can be found after the references)

Received May 6, 2011; accepted XXXX

ABSTRACT

Context. Gamma-Ray Bursts (GRBs) can provide information about star formation at high redshifts. Even in the absence of a bright optical/near-infrared/radio afterglow, the high detection rate of X-ray afterglows by *Swift*/XRT and its localization precision of 2–3 arcsec facilitates the identification and study of GRB host galaxies.

Aims. We focus on the search for the host galaxies of a sample of 17 bursts with arcsec-sized XRT error circles but no detected long-wavelength afterglow, in spite of deep and rapid follow-up observations. Three of these events can also be classified as truly dark bursts, i.e., the observed upper limit on the optical flux of the afterglow was less than expected based on the measured X-ray flux. Our goals are to identify the GRB host galaxy candidates and to characterize their phenomenological parameters.

Methods. Our study is based on deep R_C and K_s -band observations performed with FORS1, FORS2, VIMOS, ISAAC, and HAWK-I at the ESO/VLT, partly supported by observations with the seven-channel imager GROND at the 2.2-m telescope on La Silla, and supplemented by observations with NEWFIRM at the 4-m telescope on Kitt Peak. In order to be conservative, we searched for host galaxy candidates in an area with a radius twice that of the corresponding 90% c.l. *Swift*/XRT error circle.

Results. For 15 of the 17 bursts we find at least one galaxy inside the doubled XRT error circle, in two cases only a deep upper limit in R_C and K_s can be provided. In seven cases we discover extremely red objects in the error circles, at least four of them might be dust-enshrouded galaxies. The most remarkable case is the host of GRB 080207 which has a colour of $(R_C - K_s)_{AB} \sim 4.7$ mag, one of the reddest galaxies ever associated with a GRB. As a by-product of our study we identify the optical afterglow of GRB 070517A.

Conclusions. Optically dim afterglows result from cosmological Lyman drop out and dust extinction, but the former process is only required for a minority of cases ($\lesssim 1/3$). Extinction by dust in the host galaxies might explain all other events. Thereby, a seemingly non-negligible fraction of these hosts are globally dust-enshrouded, extremely red galaxies. This suggests that bursts with optically dim afterglows trace a subpopulation of massive starburst galaxies, which are markedly different from the main body of the GRB host galaxy population, namely the blue, subluminal, compact galaxies.

Key words. Gamma rays: bursts

1. Introduction

1.1. Optical afterglows

By the end of 2010, about 900 gamma-ray bursts (GRBs) have been localized at the arcmin scale (see J. Greiner's [www](http://www.greiner.net) page¹), most of them (>80%) by the *Swift* satellite (Gehrels et al. 2004). Nearly 600 events have a detected X-ray afterglow, and nearly 400 have been detected in the optical and near-infrared (NIR) bands, too. The observed brightness distribution of the optical afterglows is broad and time-dependent, spanning at least 14

magnitudes within the first hour after the burst, and at least 10 magnitudes at around 1 day, after correction for Galactic extinction (Kann et al. 2010, 2011).

In principle, the observed brightness distribution reflects the luminosity distribution of the afterglows (an intrinsic property), but it is affected by physical processes that can block the optical light on its way to the observer (external processes). The latter consists of two possible mechanisms, extinction by dust in the GRB host galaxies (GRBHs) represented by the parameter A_V^{host} , and cosmological Lyman absorption due to high redshift. If an afterglow is still detected in the optical/NIR bands, these two processes can be recognized if a redshift could be measured and a broad-band spectral energy distribution (SED) of an afterglow could be constructed. The analysis of optically detected afterglows shows that (in the R band) Lyman absorption is rather the exception than the rule; only a small fraction of bursts lies at $z \gtrsim 5$ (cf. Haislip et al. 2006; Kawai et al. 2006; Tagliaferri et al. 2005; Greiner et al. 2009; Tanvir et al. 2009; Salvaterra et al. 2009; Pérez-Ramírez et al. 2010; Cucchiara et al. 2011). In ad-

Send offprint requests to: A. Rossi, rossi@tls-tautenburg.de

[★] Based on observations collected at the Very Large Telescope of the European Southern Observatory, Paranal, Chile (ESO programmes 381.A-0647, 383.A-0399, 384.A-0414; PI: S. Klose; 081.D-0739, PI: A. Rossi, and 086.A-0533, PI: T. Krühler), GROND (PI: J. Greiner), and the Kitt Peak National Observatory (Program ID 2008B-0070; PI: A. C. Updike). Other observations are obtained from the ESO/ST-ECF Science Archive Facility.

¹ <http://www.mpe.mpg.de/~jcg/grbgen.html>

dition, it is found that while extinction by dust in GRBHs along the lines of sight is usually rather small, a long tail of possible extinction values is apparent in the data (cf. Kann et al. 2010; Greiner et al. 2011; Krühler et al. 2011), implying that at least some optical afterglows are extinguished by dust in their host galaxies.

In order to measure the redshift and the host extinction, the afterglow has to be detected in the optical bands. Even if no spectrum of the afterglow can be obtained, its precise optical localization usually means that a search for an underlying host galaxy can be undertaken and, if successful, its redshift can be measured even years after the corresponding burst. The host extinction along the line of sight can then be measured if a broad-band SED of the afterglow could be constructed. Then, in principle, the influence of Lyman dropout and host extinction on the observed SED can be distinguished from each other (e.g., Rossi et al. 2008a). However, the interplay between intrinsic luminosity, redshift, and host extinction cannot be disentangled in an easy way if no optical afterglow was detected at all.

1.2. Bursts with optically not detected afterglows

The question why a fraction of bursts has no optically detected afterglow despite a rapid localization in X-rays at the arcsec scale has been under debate since years. While many of these non-detections are simply due to the lack of rapid and deep optical follow-up observations, some events (after correction for Galactic extinction) are truly optically dark (e.g., Castro-Tirado et al. 2007; Rol et al. 2007; Hashimoto et al. 2010; Holland et al. 2010). The question then is, which of the aforementioned three physical mechanisms led to these afterglows being invisible in the optical bands.

There are two approaches to tackle this problem. On the one hand, one makes use of the theoretically expected SED of an afterglow, which allows one to predict the optical flux based on the observed X-ray flux. A comparison with observed optical upper limits can then tell if the observations simply did not probe deeply enough or if an additional dimming of the afterglow light is required (Rol et al. 2005; Jakobsson et al. 2004; van der Horst et al. 2009; Greiner et al. 2011). On the other hand, one can study the galaxy population within the corresponding X-ray error circle and try to identify the most likely GRB host candidate via statistical arguments by looking for galaxies with unusual properties. Once a putative host has been identified, not only a redshift can be constrained but also the nature of the host itself can indicate if extinction might explain the optical dimness of the afterglow light (e.g., Piro et al. 2002; Gorosabel et al. 2003; Levan et al. 2006; Berger et al. 2007; Perley et al. 2009; Küpcü Yoldaş et al. 2010). All these studies suggested that dust extinction in the GRBHs is the main reason for the optical dimness of some events. Recently, after first important steps by Cenko et al. (2009) and Perley et al. (2009), Greiner et al. (2011) settled this picture by combining rapid and deep optical with simultaneous deep NIR follow-up observations, firmly finding that optically dim afterglows are mainly due to a moderate host extinction combined with a moderate redshift ($z < 5$). The nature of the corresponding GRBHs remained to be investigated, however.

1.3. The present work

Here, we report on the results of a search for the potential hosts of a sample of 17 bursts with no detected optical/NIR after-

glow. All bursts in our sample have an observed duration in the *Swift*/BAT energy window of $T_{90} > 2$ seconds, i.e., they are classified as long GRBs (Kouveliotou et al. 1993). All events have optical upper limits well below the average brightness of detected long-GRB afterglows (Kann et al. 2010). Our goal is to identify and to study the host-galaxy candidates of these events in order to understand better which was the cause of the optical dimness of the corresponding afterglows.

Our paper is organized as follows. In section 2 we describe the sample selection and the data-reduction procedures. In section 3 we provide a detailed overview of the objects found in the corresponding *Swift*/XRT error circles. Section 4 then puts together the information about these objects and characterizes host-galaxy candidates and subsamples based on different selection criteria. Finally, a summary is given in section 5.

Throughout this work we adopt the convention that the flux density of the afterglow can be described as $F_\nu(t) \propto t^{-\alpha} \nu^{-\beta}$ and we use a Λ CDM world model with $\Omega_M = 0.27$, $\Omega_\Lambda = 0.73$, $H_0 = 71$ km/s/Mpc (Spergel et al. 2003).

2. Target selection and observations

2.1. The GRB sample

In the years from 2005 to 2008, there are about 100 bursts² with a detected X-ray afterglow but no detected optical afterglow for which declination is less than +25 deg (i.e., these fields are well observable from ESO Paranal or La Silla). From this sample we selected 17 fields with the following properties: (1) the X-ray error circle has a radius of less than 6 arcsec, (2) rapid, deep, but unsuccessful follow-up observations were performed by various optical telescopes, and (3) the Galactic visual extinction along the line of sight is less than 1 mag. In addition, at the time when we selected these targets (usually several months before they were observed) no corresponding studies had been reported in the literature.

All 17 bursts have upper limits for their optical afterglow magnitudes which lie at least 1.5 mag below the mean value of the afterglow brightness distribution (Fig. 1). The observed GRB fields are summarized in Table 1 and further details on the corresponding world-wide observing campaigns are given in Appendix A.

Deep follow-up observations of 14 of these 17 X-ray error circles were performed with VLT/FORS1, FORS2, VIMOS, ISAAC, and HAWK-I in the years 2008 to 2010, months to years after the corresponding burst (Table A.2). Limiting 3σ AB magnitudes were typically $R_C=26.5$ and $K_s=23.5$. In the case of GRBs 050717, 060211A, and 060805A, multi-band imaging was performed using GROND on La Silla and, in the case of GRBs 050922B and 060211A, data were obtained using the near-infrared imager NEWFIRM mounted at the 4-m Mayall telescope at Kitt Peak National Observatory. In the case of GRB 081204, a late *J*-band observation was executed using NTT/SOFI on La Silla.

2.2. Optical/NIR data analysis

VLT, GROND, and NEWFIRM data were reduced using IRAF tasks³ and analyzed through point-spread function (PSF) and aperture photometry using DAOPHOT and APPHOT (Tody 1993). The procedure is mainly based on the pipeline written

² <http://www.mpe.mpg.de/~jcg/grbgen.html>

³ <http://iraf.noao.edu>

Table 1: Characterization of the GRB fields of our sample.

#	GRB	T_{90} seconds	R.A., Dec. (J2000) XRT	error arcsec	Galactic coordinates (l, b) degrees	$E(B - V)$ mag
1	050717	85	14:17:24.48, -50:32:00.7	1.5	316.61, 10.04	0.238
2	050922B	150.9	00:23:13.37, -05:36:16.7	1.7	104.35, -67.45	0.037
3	060211A	126.3	03:53:32.65, +21:29:19.0	1.4	169.74, -24.40	0.192
4	060805A	5.3	14:43:43.47, +12:35:11.2	1.6	9.53, 59.97	0.024
5	060919	9.1	18:27:41.80, -51:00:52.1	1.7	343.87, -17.50	0.071
6	060923B	8.6	15:52:46.70, -30:54:13.7	1.8	342.74, 17.61	0.148
7	061102	45.6	09:53:37.84, -17:01:26.0	2.9	253.43, 28.29	0.042
8	070429A	163.3	19:50:48.92, -32:24:17.8	2.1	8.06, -25.90	0.170
9	070517A	7.6	18:30:28.93, -62:17:51.7	2.1	332.76, -21.47	0.152
10	080207	340	13:50:02.93, +07:30:07.9	1.4	340.92, 65.95	0.023
11	080218B	6.2	11:51:49.65, -53:05:48.5	1.6	293.94, 8.73	0.174
12	080602	74	01:16:42.17, -09:13:55.9	1.7	142.56, -71.13	0.028
13	080727A	4.9	13:53:33.81, -18:32:40.5	1.6	322.88, 41.91	0.073
14	080915A	14	01:11:47.63, -76:01:13.1	3.7	301.30, -41.04	0.049
15	081012	29	02:00:48.17, -17:38:17.2	1.8	185.87, -71.40	0.023
16	081105	~ 10	00:15:48.50, +03:28:15.5	4.8	105.87, -58.22	0.029
17	081204	~ 20	23:19:09.13, -60:13:31.7	5.3	321.96, -53.36	0.028

Notes: (1) The *Swift*/XRT positions for GRB 061102 and 070517A are from N. Butlers's webpage (<http://astro.berkeley.edu/~nat/swift/xrt-pos.html>) (Butler 2007). The XRT position for GRB 080915A, 081105, and 081204 are from Oates et al. (2008b), Beardmore & Cummings (2008), and Mangano et al. (2008a), respectively. All other XRT data are from <http://www.swift.ac.uk/xrt-positions/index.php>. (2) The burst duration, T_{90} , was mostly taken from <http://heasarc.gsfc.nasa.gov/docs/swift/archive/grbtable/>. For GRB 081105 the reference is Cummings et al. (2008), for GRB 080727A it is McLean et al. (2008), and for GRB 081204 it is Götz et al. (2008). (3) **The Galactic reddening along the line of sight**, $E(B - V)$, was obtained from the NASA Extragalactic Database Coordinate Transformation and Extinction calculator at <http://nedwww.ipac.caltech.edu/forms/calculator.html>.

to reduce GROND data (Yoldaş et al. 2008; Krühler et al. 2008). Aperture photometry, if not otherwise specified, was performed by using an aperture diameter of twice the Full Width Half Maximum (FWHM) of the stellar PSF. ISAAC, HAWK-I, and GROND NIR fields were calibrated using 2MASS field stars. VLT optical data were calibrated on standard star fields for the Vega photometric system, while the calibration performed for the optical $g'r'i'z'$ images of GROND employed SDSS stars (Table A.2).

3. Results

3.1. General

In the following we report the results of our deep late-time observations for each GRB field. They are summarized in Tables 2, 3, and 5. Finding charts are provided in Fig. A.1.

If not stated otherwise, in the following R_C , K_s -band magnitudes and colors are given in the AB magnitude system, in order to allow for a direct comparison with data of confirmed GRB host galaxies compiled by Savaglio et al. (2009; in the following SBG09), i.e., host galaxies which are identified via optical afterglow detections obtained with subarcsecond accuracy. All ($R_C - K_s$) colors are corrected for Galactic extinction, estimated using the extinction maps published by Schlegel et al. (1998). Thereby, we used the following transformations: (1) FORS1, FORS2, and VIMOS: $R_{AB} = R_{Vega} + 0.23$ mag (Klose et al. 2004); (2) ISAAC, HAWK-I, and NEWFIRM: $K_{AB} = K_{s,Vega} + 1.86$ mag (Klose et al. 2004). For GROND the Vega to AB conversion is $K_{AB} = K_{s,Vega} + 1.80$ mag, except for observations after an intervention on the instrument on March 2008, for which $K_{AB} = K_{s,Vega} + 1.86$ mag. Extinction corrections for the GROND

filters are: $A(g') = 1.253 A_V$, $A(r') = 0.799 A_V$, $A(i') = 0.615 A_V$, $A(z') = 0.454 A_V$, $A(J) = 0.292 A_V$, $A(H) = 0.184 A_V$, $A(K) = 0.136 A_V$, while for all other instruments we assumed the standard values $A(R_C) = 0.748 A_V$ and $A(K) = 0.112 A_V$ (Rieke & Lebofsky 1985). We always set $A_V = 3.1 E(B - V)$.

3.2. Selecting host galaxy candidates

Even in the case of arcsec-sized error boxes it is usually difficult to determine the best GRB host galaxy candidate. The approach we used here to identify a putative host is identical to the approach adopted 15 years ago, when no afterglows were known at all and at best only arcmin-sized error boxes obtained via satellite triangulation were available (e.g., Vrba et al. 1995; Klose et al. 1996; Schaefer et al. 1998; Vrba et al. 1999). The main observational difference is the size of the XRT error circles provided by *Swift*/XRT that can go down to 1-2 arcsec, allowing meaningful searches for host galaxies. The question is: Is there anything special in the field? To answer this question, we used several criteria. The first one is the magnitude-probability criterion.

Following Bloom et al. (2002) and Perley et al. (2009), we calculated, for every object, the probability p of finding a galaxy of any type of the given (extinction-corrected) R_C -band magnitude m in a region of radius r , where r is the radius of the associated error circle. It is

$$p(m) = 1 - \exp(-\pi r^2 \sigma(\leq m)), \quad (1)$$

where $\sigma(\leq m)$ is the surface density of galaxies with magnitudes $\leq m$ (equation 3 in Bloom et al.). If the object we have found is located within the 90% c.l. XRT error circle of radius

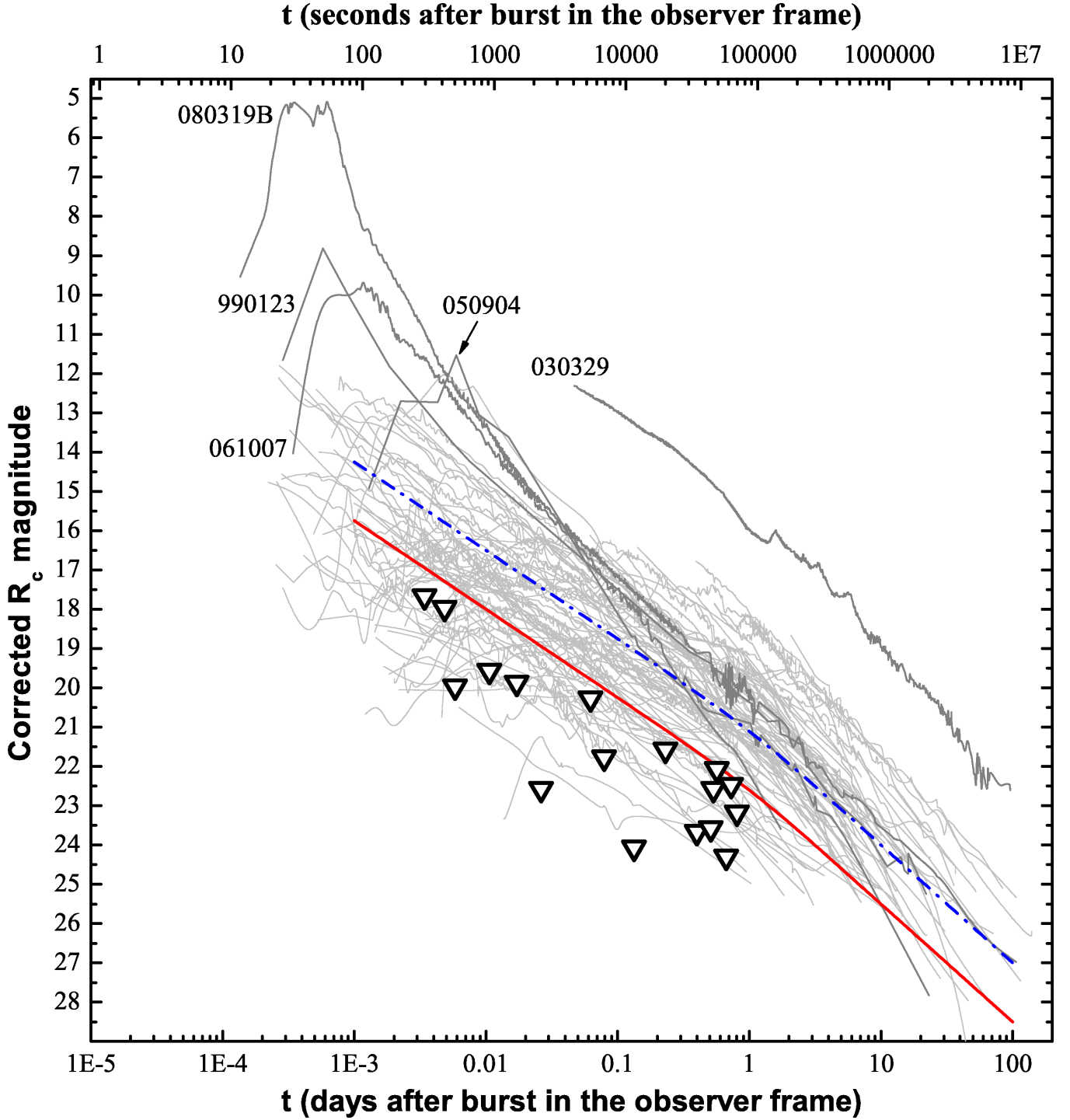


Fig. 1: The R_C -band light curves of all (long) afterglows in the sample of Kann et al. (2010, 2011). All data have been corrected for Galactic extinction. Triangles indicate equivalent R_C -band upper limits of the afterglows in our sample (Table 4). The blue dashed/dotted line approximately indicates the mean of the afterglow brightness distribution. The red line indicates the border line of all targets in our study.

r_0 , we set $r = r_0$, if it is placed within $[(n-1)r_0, nr_0]$, then we set $r = nr_0$. The input for $\sigma(\leq m)$ is the relation derived by Hogg et al. (1997), which is based on galaxy counts down to about $R_{\text{Vega}} = 26.5$. We consider galaxies of all types as very likely GRB host galaxy candidates if the chance probability p to find such an object of the given R_C -band magnitude in the corresponding error circle is $\leq 10\%$ (within 1σ).

More powerful criteria rely on the phenomenological appearance of the galaxies, in particular their color. Spiral galaxies have a maximum $(R-K)_{\text{AB}}$ color of about 3.5 mag before the Lyman dropout at high z comes into play (SBG09; their figure 3). Galaxies with a larger $(R-K)_{\text{AB}}$ color are therefore of special interest, since it can either point to a dust-enshrouded or to a Lyman-dropped-out galaxy. These galaxies are usually called extremely red objects (EROs) and they were first addressed in

the context of deep NIR surveys (Elston et al. 1988). Number counts of these galaxies are available now (Gonzalez-Perez et al. 2009; Hempel et al. 2011; Kim et al. 2011) and will be used in the following also. Finding an ERO galaxy in an XRT error circle is considered as strong evidence that this object is related to the burst under consideration. The ERO galaxies population follows a bimodal distribution and differentiates between passively evolving ellipticals and dusty star-forming galaxies in the redshift interval $1 \lesssim z \lesssim 2$ (Doherty et al. 2005; Fontanot & Monaco 2010; Gonzalez-Perez et al. 2011). Long GRBs then naturally select star-forming galaxies. Given that the ratio between both populations is still a matter of detailed studies (see Conselice et al. 2008; Gonzalez-Perez et al. 2009; Kong et al. 2009; Fontanot & Monaco 2010), any statistics based on ERO number counts then provide a conservative upper limit on the probability to find a star-forming ERO galaxy in a *Swift*/XRT error circle.

Finally, also a close pair of galaxies inside an XRT error circle, i.e., a hint of interaction and thus triggered star-formation, is a good candidate for the birthplace of a (long) GRB progenitor.

3.3. Notes for individual targets

GRB 050717 The burst occurred at relatively low Galactic latitude ($b = 10^\circ$), and the field is relatively crowded with stars. The foreground Galactic reddening is moderate, $E(B - V) = 0.24$ mag, the highest in our sample. The 90% c.l. XRT error circle has a radius of $r_0 = 1''.5$ (see the combined GROND $r'i'z'$ -band image, Fig. A.1).

We observed the field with GROND two years after the burst. Within $2r_0$ two objects (A and B) are visible in the combined $r'i'z'$ -band image (Fig. A.1). Object A ($R_{AB} = 23.6$) lies outside $1r_0$, appears fuzzy and has a size of about $2''.1 \times 3''.9$. Based on its visual appearance this is a faint galaxy. Its outer parts extend into the 90% c.l. error circle. The fainter object B ($R_{AB} = 24.5$) lies within $1r_0$ close to the southern boundary of the error circle. Neither object is detected in g' and also not seen in the NIR bands (Table 3). Given the non-detection in the NIR ($K_{AB} > 22.1$), for both objects only an upper limit for $(R - K)_{AB}$ can be given (< 2.6 mag and < 3.4 mag, respectively).

Assuming that A and B are galaxies, the probability p of finding a galaxy of the given R_C -band magnitude in a region of radius $2r_0$ and $1r_0$ is about 0.05 and 0.03, respectively. Therefore, we consider both objects as equally likely GRB host galaxy candidates.

GRB 050922B The burst occurred at high Galactic latitude ($b = -67^\circ$); the field is not crowded with stars. The foreground Galactic reddening is very small, $E(B - V) = 0.04$ mag. The 90% XRT error circle has a radius of $r_0 = 1''.7$ (Fig. A.1). The field was observed with NEWFIRM in the K_s -band about 3 years after the burst. Additional data were obtained with FORS2 and ISAAC one year later. No object is found in any band, neither within the 90% c.l. XRT error circle nor within $2r_0$, down to deep 3σ upper limits of $R_{AB} > 26.5$ and $K_{AB} > 22.8$.

GRB 060211A The field of GRB 060211A lies at relatively low Galactic latitude ($b = -24^\circ$) but it is not crowded with stars. The foreground Galactic reddening is moderate, $E(B - V) = 0.19$ mag. The 90% c.l. XRT error circle has $r_0 = 1''.4$ (Fig. A.1).

We observed the field 1.5 and 3 years after the burst with GROND and NEWFIRM (J and K), respectively. In the 90%

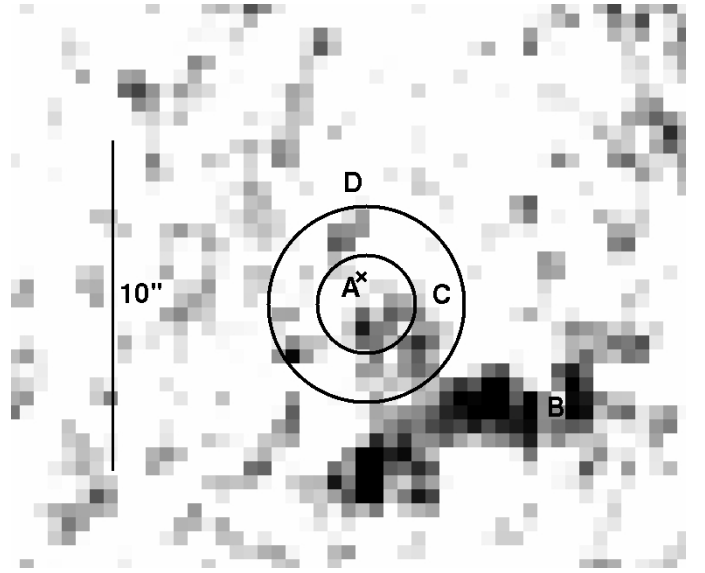


Fig. 2: NEWFIRM J -band image of the field of GRB 060211A. It shows the 90% c.l. XRT error circle ($r_0 = 1''.4$) as well as a circle of radius $2r_0$. The cross indicates the position of object A which is visible in the GROND r' -band image (Fig. A.1).

c.l. error circle we find one object (A) in the GROND r' band, which looks slightly extended in N-S direction ($1''.1 \times 1''.2$). The object is not visible in the other GROND bands. Complementary NEWFIRM observations did not detect this object down to $J_{AB} = 23.6$ and $K_{AB} = 21.6$ either. Therefore, only an upper limit on the $(R - K)_{AB}$ color of object A can be given (< 2.5 mag).

In addition to A, an extended, fuzzy object (B) is detected with GROND in $g'r'i'z'$, and located about $4''.0$ ($3r_0$) away from the center of the error circle (see Fig. A.1). This object is also seen in the NEWFIRM J -band image, where it appears resolved into two or three sources (Fig. 2). In the r' band its size is about $3''.8 \times 2''.2$.

The NEWFIRM J -band image reveals other two very faint sources, C and D (Fig. 2). Object C ($J_{AB} \sim 23.1$) is an extended object lying within the 90% c.l. error circle. This potential host galaxy is not seen in any other band. Object D ($J_{AB} \sim 23.4$) is outside the 90% c.l. error circle and it is too faint for any conclusion about its morphology and nature. The angular offset of D from the boundary of the 90% c.l. error circle is $0''.7$. For a redshift of 1 or 0.5 this would correspond to a projected distance of 5.6 kpc and 4.3 kpc, respectively. This is still a reasonable value (Bloom et al. 2002). Unfortunately, we cannot decide if objects C and D are potential ERO galaxies: An ERO would have an $(r' - J)_{AB}$ color of at least 2 mag, fainter in r' than our GROND detection limit. Assuming that A is a single galaxy, the probability p of finding a galaxy of the measured R_C -band magnitude within the 90% c.l. error circle is about 0.03, while the corresponding value for object B is 0.08. We conclude that in this case we cannot decide which is the best host galaxy candidate; it can be A, B, C, or D.

GRB 060805A The field lies at relatively high Galactic latitude ($b = 60^\circ$). It is not crowded with stars but it is located close to a bright star ($R_C = 13.5$) at RA, Dec. (J2000) = 14:43:42.098, +12:35:20.63 (USNO-B1 catalog), which may affect the background estimation. The foreground Galactic reddening is small,

$E(B - V) = 0.02$ mag, among the smallest in our sample. The corresponding 90% c.l. XRT error circle has $r_0 = 1''.6$ (Fig. A.1).

The field was observed with GROND two years after the burst. In the r' -band image we detect two sources (A, B; Fig. A.1) inside $1r_0$ and $2r_0$ with magnitudes $R_{AB} = 25.0$ and 23.6, respectively. Both objects appear extended. Object B, with a size of $2''.7 \times 1''.3$, lies about $2''.0$ away from the center of the XRT error circle but its outer regions extend into it. Contrary to object A, object B is also detected in the g' -band (~ 23.6) with a $(g' - r')_{AB}$ color consistent with a flat SED in this wavelength region. It could imply that this galaxy is dominated by a young stellar population. Both objects are not detected in the GROND $i'z'JHK_s$ bands, where only deep upper limits could be derived (Table 3). The $(R - K_s)_{AB}$ colors of A and B are < 4.3 mag and < 2.6 mag, respectively.

Assuming that A and B are galaxies, the probability p of finding a galaxy of the measured R_C -band magnitude within $1r_0$ and $2r_0$, respectively, is about 0.06 for object A and 0.09 for object B. We consider both, A and B, as GRB host galaxy candidates. The same conclusion was drawn by Perley et al. (2009), who observed this field in g' and R_C using the Keck telescopes.

GRB 060919 The field of this burst lies at low Galactic latitude ($b = -17^\circ$) but is not crowded with stars. The foreground Galactic reddening is small, $E(B - V) = 0.07$ mag, and the 90% c.l. XRT error circle is among the smallest in our sample ($r_0 = 1''.7$; Fig. A.1).

The field was observed with FORS1 and ISAAC about 2 years after the burst in R_C and K_s , respectively. We find only a single R_C -band source within the 90% c.l. error circle (object A; Fig. A.1), with $R_{AB} = 26.1$. No other objects are visible even within $2r_0$. In the R_C -band image object A seems to be extended along the E-W direction ($1''.5 \times 1''.4$). It is not detected in the ISAAC image down to deep flux limits ($K_{AB} > 23.4$). Its $(R - K)_{AB}$ color is thus < 2.6 mag, well within the range of the colors of the known GRB host galaxy population (SBG09). If this object is not the host, then we can provide the following upper limits for the GRB host galaxy: $R_{AB} > 26.5$ and $K_{AB} > 23.4$.

The probability of finding a galaxy of the measured R_C -band magnitude in a region of radius $1r_0$ is 0.15. Given that object A is the only object we detect within $2r_0$, we suggest that it is the potential GRB host galaxy.

GRB 060923B The field lies at relatively low Galactic latitude ($b = 18^\circ$) and it is relatively crowded with bright stars. The foreground Galactic reddening is moderate, $E(B - V) = 0.15$ mag. The corresponding 90% c.l. XRT error circle has $r_0 = 1''.8$ (Fig. A.1).

We observed the field with FORS1 and ISAAC about 1.5 years after the burst. Our FORS1 R_C -band as well as our ISAAC K_s -band observations show two objects (E and C; Fig. A.1) at the inner border of the 90% c.l. error circle, while three more objects (A, B, and D) lie within $2r_0$.

Objects A ($R_{AB} = 23.1$) and E are very close to each other, making it difficult to get a reliable R -band photometry, especially for object E. Object B ($R_{AB} = 21.7$), has a PSF that is point-like. On the deep K_s -band image object A shows an extended morphology ($2''.2 \times 2''.1$; Fig. 3). Object C ($R_{AB} \sim 24.5$) has a point-like PSF but it is probably too faint for detecting the faintest region of a galaxy. Object D appears slightly elongated in the optical and the NIR images, but it is too faint for any conclusion about its morphology. Therefore, with high confidence only object A can be identified as a galaxy.

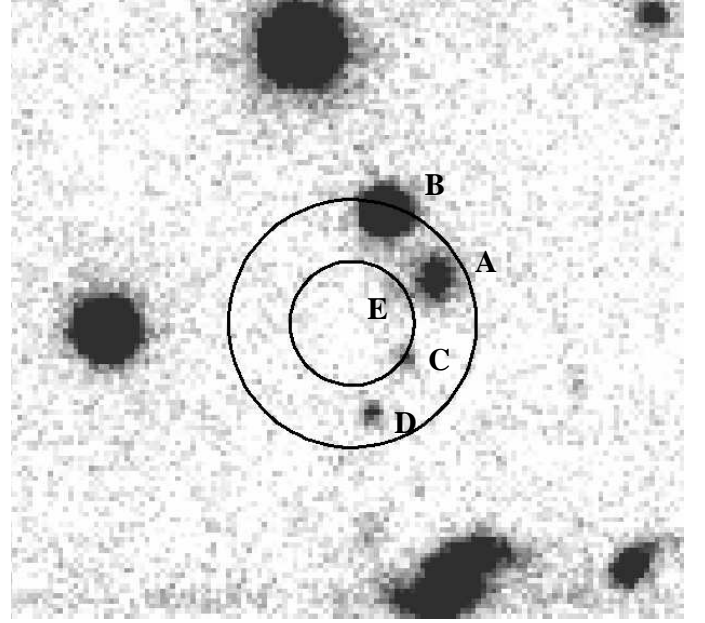


Fig. 3: ISAAC K_s -band image of the field of GRB 060923B. Also shown is the 90% c.l. XRT error circle ($r_0 = 1''.8$) as well as a circle of radius $2r_0$. The image reveals that object A is a galaxy. Object D is an ERO.

The probability p of finding a galaxy like A of the measured R -band magnitude inside a region of radius $2r_0$ is 0.06. Objects C and E have p -values of less than⁴ 0.1, but it is difficult to conclude anything about their nature. If E is a galaxy it would be attractive, because of its position close to galaxy A, suggesting a possible interaction. On the other hand, Object D ($R_{AB} = 25.7$) is an ERO with $(R - K)_{AB} \sim 3.8$ mag, while A and C have a modest color of 1.1 mag and 1.3 mag, respectively.

Given that we can only say with confidence that object A is a galaxy, and given that D could be an ERO galaxy, we consider A and D as the most likely host galaxy candidates (see Sect. 4.8).

GRB 061102 The field lies at moderate Galactic latitude ($b = 28^\circ$). The foreground Galactic reddening is small, $E(B - V) = 0.04$ mag. The corresponding 90% c.l. XRT error circle has a radius of $r_0 = 2''.9$ (Fig. A.1).

We observed the field with FORS1 and ISAAC in R_C and K_s , respectively, about 1.5 years after the burst. The VLT images show no object within the 90% c.l. error circle down to $R_{AB} = 26.9$ and $K_{AB} = 22.8$. Two objects (A, B) are found within $2r_0$ (Fig. A.1). They are only detected in R_C but not in K_s . Both objects are clearly extended ($2''.5 \times 1''.5$ and $1''.8 \times 1''.9$, respectively). Their $(R_C - K_s)_{AB}$ color (≤ 1.2 mag and ≤ 1.1 mag, respectively) matches with the corresponding color of the GRB host galaxy population at a redshift around $z = 1$ (SBG09). In both cases, the probability of finding a galaxy of the given R_C -band magnitude inside a region of $2r_0$ is 0.3.

Object A touches the 90% c.l. error circle, while the brightness center of object B lies $2''.0$ away. However, B is surrounded by a faint, asymmetric halo structure, which extends down to $1r_0$. We speculate that this could be a face-on spiral galaxy or the tidal tail of an interacting system. If B lies at a redshift of, say, $z = 0.3$ or 0.5 , the projected offset of the afterglow from the center of this galaxy would be 9 kpc and 12 kpc, respectively.

⁴ assuming for E a conservative $R = 24.5 \pm 0.5$ gives $p = 0.05 \pm 0.02$

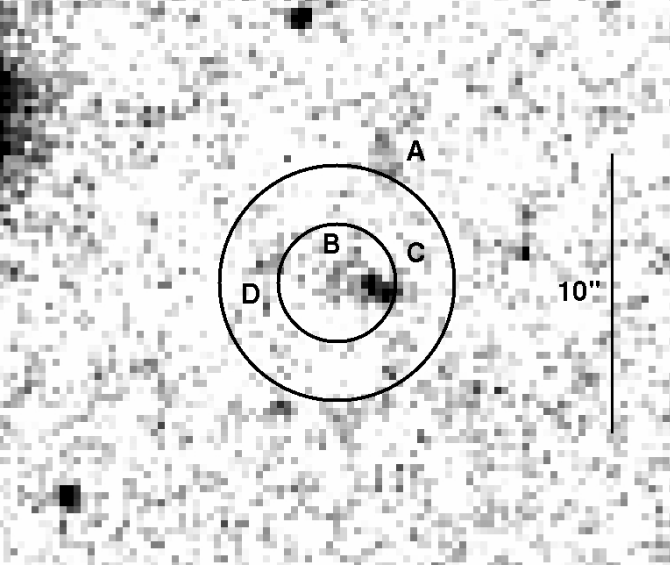


Fig. 4: ISAAC K_s -band image of the field of GRB 070429A. Also shown is the 90% c.l. XRT error circle ($r_0 = 2''.1$) as well as a circle of radius $2r_0$. Together with objects A, B and C, the image reveals object D, which is not visible in the FORS1 R_C -band image. Object D is an ERO.

This is a very large offset. It can be reduced if the redshift is notably smaller, which would then point to a rather subluminal galaxy (see also Sect. 4.6 and Table A.3).

If none of these sources is the host galaxy, then the measured deep R_C and K_s -band upper limits would make the host galaxy of GRB 061102 one of the faintest in our sample.

GRB 070429A The field lies at moderate Galactic latitude ($b = -26^\circ$). It is not crowded with stars. The foreground Galactic reddening is modest, $E(B - V) = 0.17$ mag. The corresponding 90% c.l. XRT error circle has $r_0 = 2''.1$ (Fig. A.1).

We observed the field with FORS1 and ISAAC about 1 year after the burst. In the FORS1 R_C -band image (Fig. A.1) we find one object (A) at $2r_0$ and two other sources inside the 90% c.l. error circle (B,C), with R_C -band magnitudes of 25.0 ± 0.2 , 24.1 ± 0.1 , and 24.3 ± 0.1 , respectively. In the ISAAC K_s -band images another object is visible (D, $K_s = 23.0 \pm 0.4$, Fig. 4). All four objects are extended (between $1''.6$ and $3''.8$ in their major axis). Objects B and C could be an interacting pair since they show a fuzzy structure. The individual R_C , K_s magnitudes of objects A, B and C (in $K_s = 22.4 \pm 0.2$ and 21.9 ± 0.1 , respectively; Table 2) and $(R - K)_{AB}$ colors (Table 5) are compatible with the GRB host population at a redshift $z < 2$ (SBG09). Therefore, the observed color of objects A, B, and C does not characterize any of them as very red. However, object D is very red ($(R - K)_{AB} > 3.1$ mag). Even though D has a large 0.4 mag error in the K_s -band photometry, we consider it as a potential ERO galaxy. Its center lies outside $1r_0$, but its outskirts reach into the 90% c.l. error circle.

The probability-magnitude criterion gives the following numbers for the first three galaxies (A-C): 0.54, 0.04 and 0.05, respectively. Given that B and C are well placed inside the 90% c.l. error circle, have low p -values and are probably an interacting galaxy system, we consider both as equally likely host galaxy candidates. In addition, D is also a host galaxy candidate given its very red color.

GRB 070517A This burst is unique in our sample, because we could identify its afterglow by comparing our late-time observations with the follow-up observations reported by Fox et al. (2007).

We observed the field with FORS1 and ISAAC about 1 year after the burst. The field is at relatively low Galactic latitude ($b = -21^\circ$) but not very crowded with stars. The foreground Galactic reddening is modest, $E(B - V) = 0.15$ mag. The corresponding 90% c.l. XRT error circle has $r_0 = 2''.1$ (Fig. A.1).

In the R_C -band image we detect only one object (A, Fig. A.1) inside the 90% c.l. XRT error circle with magnitudes $R_{AB} = 25.39 \pm 0.21$ and $K_{AB} > 23.4$. No further objects are apparent within the doubled XRT error circle ($r = 2r_0$). In particular, we do not detect the $r' = 22.1$ afterglow candidate at RA, Dec. (J2000) = $18:30:29.12$, $-62:17:50.7$ (uncertainty of $< 0''.75$ in each coordinate), which was reported by Fox et al. (2007) based on Gemini-South observations about 16 hr after the burst (indicated by a cross in Fig. A.1). We conclude that in fact this was the GRB afterglow.

The coordinates of object A agree with the second object detected by Fox et al. (2007) at RA, Dec. (J2000) = $18:30:29.08$, $-62:17:53.0$ with $i' = 24.5$. Based on our images, we conclude that A is a galaxy. Its angular size is $1.6'' \times 1.3''$, which is ~ 2 times that of the stellar FWHM. If it is the GRB host galaxy, then its $(R - K)_{AB}$ color of < 1.7 mag is compatible with the GRB host galaxy population for a redshift around $z = 1$ (SBG09). No underlying galaxy is found at the position of the optical afterglow down to $R_{AB} = 26.6$ and $K_{AB} = 23.4$.

The angular distance between the afterglow and object A is $1''.6 \pm 0''.3$. The probability p to find a galaxy of the given R_C -band magnitude in a circle with this radius is between 0.04 and 0.10. If A were the host galaxy of GRB 070517A, then its angular distance translates to a projected distance of 12.8 ± 2.4 kpc, assuming a redshift of $z = 1$. This is 10 times larger than the median projected angular offset of 1.3 kpc found by Bloom et al. (2002) for a sample of 20 host galaxies of long bursts, leading to object A to not be favored as a host. On the other hand, if we require a projected angular distance of less than 10 kpc, then the upper limit on the redshift of this galaxy is $z = 0.4$. In this case A would be a very faint galaxy when compared to the sample of SBG09. Alternatively, the true host galaxy could underlie the optical afterglow position below our detection limits. We conclude that in the case of GRB 070517A we have no good host galaxy candidate.

GRB 080207 The burst occurred at high Galactic latitude ($b = 66^\circ$), the field is not crowded with stars. The Galactic reddening is very small, $E(B - V) = 0.02$ mag. The 90% c.l. XRT error circle is the smallest in our sample ($r_0 = 1''.4$; Fig. A.1).

We observed the field 2 years after the burst with VLT/VIMOS in R_C and ISAAC in K_s . In addition, deep GROND imaging was performed at a mean time of 10 hours after the burst, but no afterglow was detected (Table A.1). Our deep VIMOS R_C -band image shows one fuzzy object ($2''.4 \times 1''.3$) at the north-east boundary of the 90% c.l. error circle (A, Fig. A.1). This object is very faint in the K_s -band. In addition, the ISAAC image shows another, elongated source (B; $1''.6 \times 0''.9$; Fig. 5) within the XRT error circle that has a very faint R_C -band counterpart with $R_{AB} \sim 26.5$. GROND did not detect these sources in any band, only upper limits can be provided (Table 3). Object B is very red, $(R - K)_{AB} = 4.7$ mag. Its color and morphology defines it as an ERO galaxy. Given its position within the 90%

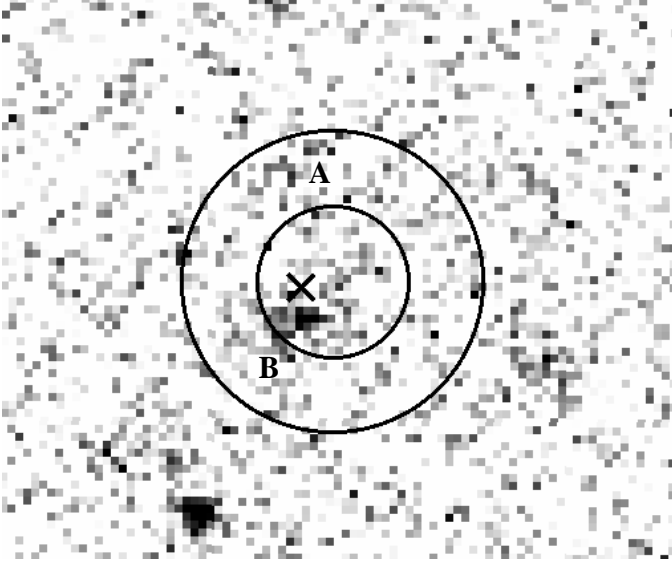


Fig. 5: ISAAC K_s -band image of the field of GRB 080207, including the 90% c.l. XRT error circle ($r_0 = 1''.4$) as well as a circle of radius $2r_0$. Object A is only visible in the VLT/VIMOS R_C -band image (Fig. A.1). Also shown by a cross is the position of the *Chandra* X-ray source. Object B is an ERO.

c.l. error circle, we consider B as the most likely GRB host candidate.

When this paper was in its finalization, the *Chandra* source catalogue (Evans et al. 2010) became public. Inspection of the catalogue shows that a X-ray observation of the field was performed 8 days after the burst and a point source was detected (CXO J135002.9+073007) at coordinates RA, Dec. (J2000) = 13:50:02.97, 07:30:07.8 ($\pm 0''.6$). The position of this source is within 1σ consistent with the position of object B. Therefore, we conclude that this is the host galaxy of GRB 080207. Hunt et al. (2011) have recently obtained a photometric redshift of about 2.2 for this galaxy.

GRB 080218B The field is at relatively low Galactic latitude ($b = 9^\circ$), the lowest in our sample. However, it is only moderately crowded with stars. The Galactic reddening along the line of sight is modest, $E(B - V) = 0.17$ mag. The 90% c.l. XRT error circle has $r_0 = 1''.6$ (Fig. A.1).

We observed the field with FORS2 and ISAAC about 1 year after the burst. In addition, deep GROND imaging was performed at a mean time of about 0.75 hr after the burst, but no afterglow was detected (Table A.1). Our deep FORS2 R_C -band image reveals one faint ($R_{AB} = 26.2$), extended object (A) within the 90% c.l. error circle and another object (B; $R_{AB} = 24.6$) inside $3r_0$. Both objects are also detected with ISAAC at magnitudes $K_{AB} = 21.7$ and 22.7 , respectively (Fig. 6). Object A is too faint to be detected by GROND, while B is detected in $g'r'z'$ (Table 3; it is not seen in i' due to ghost images in the field).

In the FORS image object A is elongated in SW-NE direction ($2''.5 \times 1''.1$). It could be a spiral galaxy seen nearly edge-on or a tight pair of galaxies. If it is a single galaxy, then its large $(R - K)_{AB}$ color (4.2 mag) defines it as an ERO galaxy. The probability of finding a galaxy of this R_C -band magnitude within an area of radius $1r_0$ on the sky is about 0.1. Given its extremely red color and its position inside the 90% c.l. error circle, we consider A as the most likely GRB host galaxy.

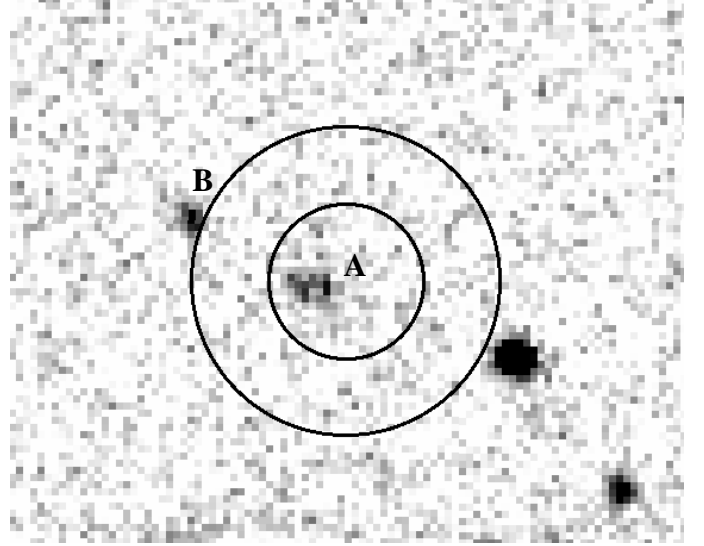


Fig. 6: ISAAC K_s -band image of the field of GRB 080218B, including the 90% c.l. XRT error circle ($r_0 = 1''.6$) as well as a circle of radius $2r_0$. Object A is an ERO.

GRB 080602 The field is at high Galactic latitude ($b = -71^\circ$), among the highest in our sample. The Galactic reddening is very small, $E(B - V) = 0.03$ mag. The 90% c.l. XRT error circle has $r_0 = 1''.7$ (Fig. A.1).

We retrieved VLT/FORS2 and ISAAC data obtained about 1 year after the burst from the ESO archive (program ID 081.A-0856; PI: P. Vreeswijk). In addition, deep GROND multi-color imaging was performed 1.5 years after the burst. In the FORS2 R_C -band image we find one object (A; $R_{AB} = 22.9$) inside the 90% c.l. error circle. It is also detected in all GROND optical bands and also seen in the ISAAC K_s -band image ($K_{AB} = 22.5$), where it seems to split into two objects, with the second one (C) $1''.3$ north of A (Fig. 7). Even though in the FORS image object A looks extended in the northern direction, C has no direct optical counterpart: The angular distance between A and C on the ISAAC image is larger by about $0''.5$ than the distance between the brightness center of A and its fainter northern blob on the FORS image. Therefore, we consider C as a separate object. Its $(R - K)_{AB}$ color (>4.3 mag) defines it as an ERO.

At the southern boundary of the 90% c.l. error circle lies another object (B; size $2''.0 \times 1''.8$; Fig. A.1), possibly another galaxy. In both R_C and K_s -band images, object A looks fuzzy and extended ($2''.6 \times 2''.0$), while the nature of C is less obvious. Assuming that A (including its northern blob) is a single galaxy, a fit of its SED with *Hyperz* (Bolzonella et al. 2000) gives good solutions for a spiral galaxy with no intrinsic extinction at a redshift of $z = 1.40^{+0.30}_{-0.15}$ ($\chi^2/\text{d.o.f} = 0.074$) as well as for a starburst galaxy at a redshift of $z = 2.10^{+0.20}_{-0.35}$ and a moderate Milky Way (MW) extinction of $A_V = 0.4$ mag ($\chi^2/\text{d.o.f} = 0.050$; Fig. 8). This double solution is due to the fact that the z' -band magnitude can well fit both the 4000Å Balmer jump as well as a moderate 2175Å feature from a MW (or LMC) extinction law. We caution, however, that while the first solution implies an absolute magnitude $M_B \sim -23.0$, in the case of the $z \sim 2.1$ solution we obtain $M_B \sim -24.0$, which is very unlikely when compared to the luminosity function found in the Las Campanas redshift survey (Lin et al. 1996). Therefore, we consider $z = 1.4^{+0.30}_{-0.15}$ as the most likely redshift estimation.

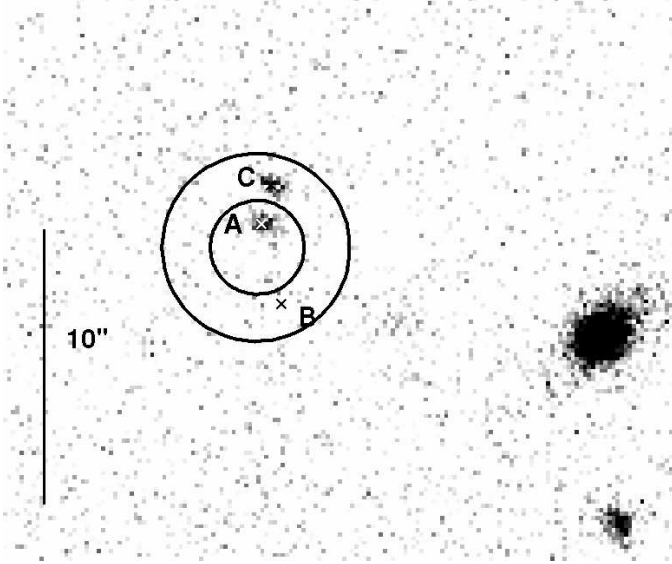


Fig. 7: ISAAC K_s -band image of the field of GRB 080602, including the 90% c.l. XRT error circle ($r_0 = 1''.7$) as well as a circle of radius $2r_0$. Object C is an ERO. The crosses show the positions of objects A and B in the FORS image (Fig. A.1).

Object A as well as B have colors $(R - K)_{AB} = 0.3$ mag and < 0.4 mag, respectively, which is well within the range of the observed colors for GRB host galaxies (SBG09). In the case of object A, the probability of finding a galaxy of the given R_C -band magnitude inside a circular area of radius $1r_0$ is 0.01, while for B the corresponding value is 0.13 (within $2r_0$). However, the probability to find an ERO (object C) within the same area is much smaller (see Sect. 4.8). Therefore, we consider object C as well as its possible interacting partner A as the most likely host galaxy candidates.

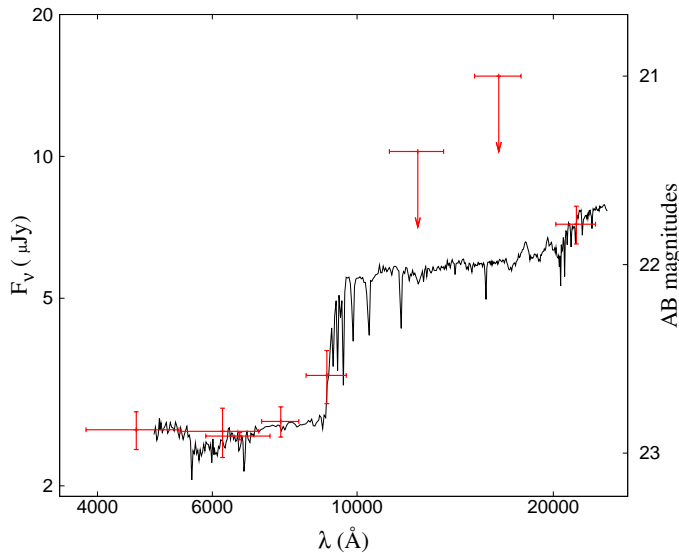


Fig. 8: *Hyperz* best-fit solution of the broad-band SED of object A in the XRT error circle of GRB 080602. The fit suggests a spiral galaxy at a redshift of $z = 1.40^{+0.30}_{-0.15}$ with no intrinsic extinction ($\chi^2/\text{d.o.f} = 0.074$).

GRB 080727A The field lies at moderate Galactic latitude ($b = 42^\circ$) and is not crowded by stars. The Galactic reddening is very small, $E(B - V) = 0.07$ mag. The 90% c.l. XRT error circle has $r_0 = 1''.6$ (Fig. A.1).

We observed the field with ISAAC about 1.5 years after the burst. The deep FORS1 R_C -band image was taken from the ESO archive (program ID 081.A-0856; PI: P. Vreeswijk; FWHM of $0''.8$). No GRB host galaxy is detected inside $2r_0$, down to $R_{AB} = 26.3$ and $K_{AB} = 23.0$. This is the second case (besides GRB 050922B) in our sample where only deep upper limits can be provided for the GRB host galaxy within $2r_0$. A moderately bright, nearly edge-on galaxy ($R_{AB} = 23.4$; size $4''.5 \times 2''.0$) lies $10''$ east of the center of the XRT error circle. This object lies too far away from the XRT error circle in order to be physically related to the GRB.

GRB 080915A The field does not lie at low Galactic latitude ($b = -41^\circ$), but it is relatively crowded with stars. The Galactic reddening is very small, $E(B - V) = 0.05$ mag. The 90% c.l. XRT error circle is of median size ($r_0 = 3''.7$; Fig. A.1).

The field was observed in the K_s -band with HAWK-I in Target of Opportunity mode starting 28 hours after the burst, lasting for 14 minutes. No candidate NIR afterglow was found inside $2r_0$ down to $K_{AB} = 23.4$. The HAWK-I observations reveal two bright objects, one (A) within the 90% c.l. error circle and one (B) just outside $2r_0$ with AB magnitudes 20.42 ± 0.02 and 19.19 ± 0.01 , respectively (Fig. 9). These objects were also detected with GROND in all bands during the same night (Table 3). Additional R_C -band data were obtained with FORS1 12 days after the burst (FWHM of $1''.4$). The FORS image shows objects A ($R_{AB} = 21.47 \pm 0.01$) and B ($R_{AB} = 21.12 \pm 0.01$), but also reveals the presence of three additional objects: C ($R_{AB} = 24.55 \pm 0.07$) and E ($R_{AB} = 25.28 \pm 0.15$) within $1r_0$ as well as D ($R_{AB} = 24.41 \pm 0.08$) slightly outside $1r_0$ (Fig. A.1).

In the FORS image object A has a PSF that is compatible with a point source, while C and D appear fuzzy and could be galaxies. Object E is very faint, close to the detection limit. It is difficult to decide if it is a galaxy or not. Object B, just outside $2r_0$, is a galaxy ($5''.6 \times 4''.5$ in the FORS1 image), with a relatively large $(g' - r')_{AB}$ color of 2.0 mag.

For objects C and D the probability of finding a galaxy with the corresponding R_C -band magnitude inside a circle of radius $1r_0$ and $2r_0$ on the sky is $p = 0.08$ and 0.35, respectively. Given that this could be an interacting pair, which partly extends into the 90% c.l. error circle, we consider both as GRB host galaxy candidates.

GRB 081012 The field is at high Galactic latitude ($b = -71^\circ$), it is not crowded with stars. The Galactic reddening is very small, $E(B - V) = 0.02$ mag, among the lowest in our sample. The 90% c.l. XRT error circle has $r_0 = 1''.8$ (Fig. A.1).

We observed the field with VIMOS and ISAAC about 1 year after the burst. Our deep VIMOS R_C -band image shows no source within the 90% c.l. error circle down to $R_{AB} = 26.7$. One object (A, Fig. A.1) is detected between $1r_0$ and $2r_0$. It has a cometary shape ($1''.8 \times 1''.5$) and a magnitude of $R_{AB} = 25.16 \pm 0.17$. It is possible that this is an irregular galaxy or a galaxy with a Galactic foreground star superposed its southern part. The object is not visible in our ISAAC image down to $K_{AB} = 23.9$. This yields an upper limit of $(R - K)_{AB} < 1.2$ mag, but given the potential foreground star, this color should be considered with caution. The field was also observed by GROND while searching for the afterglow at a mean time of 19.3 hr after

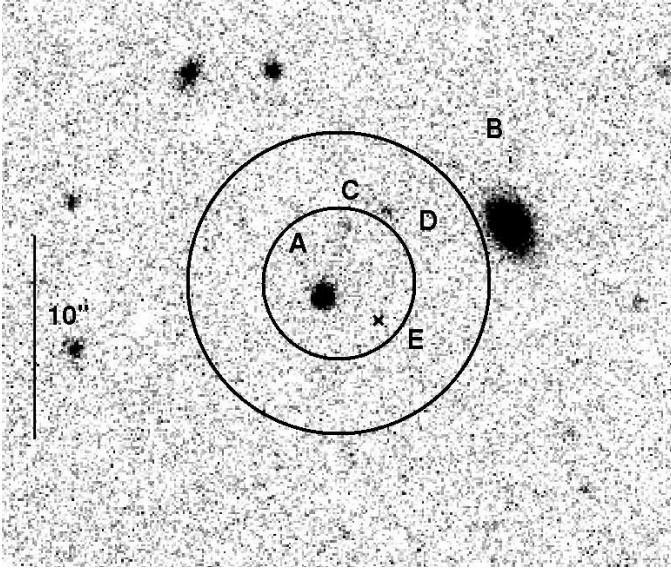


Fig. 9: Deep VLT/HAWKI K_s -band image of the XRT error circle of GRB 080915A taken 28 hr after the burst. Also shown is the 90% c.l. XRT error circle ($r_0 = 3''.7$) as well as a circle of radius $2r_0$. Here object E is not visible and therefore it is indicated by a cross. All objects are also detected in a deep VLT/FORS1 image taken 11 days later.

the burst. Neither object A nor any transient source were detected in any band (Filgas et al. 2008; Tables 3, A.1).

Given the absence of any other source within the 90% c.l. error circle, object A ($p = 0.3$) is the only host galaxy candidate, even though it is a weak candidate: The angular offset of A from the boundary of the 90% c.l. error circle is $1''.0$. For a redshift of $z = 1$ or 0.5 this would correspond to a projected distance of 8.0 kpc and 6.0 kpc, respectively. This is a relatively large value (Bloom et al. 2002). If object A is not the host, then the GRB host galaxy is fainter than $R_{AB} = 26.7$ and $K_{AB} = 23.9$.

GRB 081105 The field is at moderately high Galactic latitude ($b = -58^\circ$), not very crowded by stars. The Galactic reddening is very small, $E(B - V) = 0.03$ mag. The 90% c.l. XRT error circle has $r_0 = 4''.8$ (Fig. A.1).

We observed the field with VIMOS and ISAAC about 1 year after the burst. In spite of the relatively large size of the XRT error circle, in the deep VIMOS R_C -band image we detect only two objects A and B, with AB magnitudes 23.65 ± 0.08 and 24.26 ± 0.13 respectively (Fig. A.1). Both objects are also visible in the deep ISAAC K_s -band image, with AB magnitudes 22.78 ± 0.18 and 22.13 ± 0.14 , respectively. In the ISAAC image object A splits into two separate objects, with the second one (C; $K_{AB} = 21.74 \pm 0.13$) $1''.0$ south of A (Fig. 10). This object C is an ERO ($(R - K)_{AB} > 3.5$ mag). In the K_s -band image objects A and C appear slightly extended, i.e., these might be (interacting) galaxies. In case of B we cannot determine if it is a star or a galaxy.

The field was also observed by GROND while searching for the afterglow, starting about 13 hr after the burst. No transient source was detected in any band, only deep upper limits could be obtained (Clemens et al. 2008; Table A.1). None of the three objects (A,B,C) was detected (Table 3).

The $(R - K)_{AB}$ colors of objects A and B (about 0.9 mag and 2.1 mag, respectively) match those of the sample of GRBHGs at

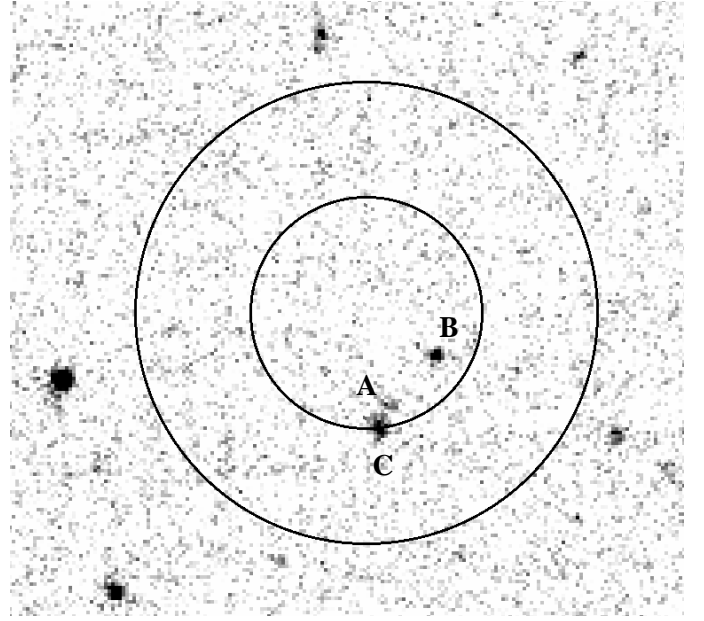


Fig. 10: ISAAC K_s -band image of the field of GRB 081105. Also shown is the 90% c.l. XRT error circle ($r_0 = 4''.8$) as well as a circle of radius $2r_0$. Object C is an ERO.

a redshift around $z = 1$ (SBG09). The probability of finding a galaxy with the R_C -band magnitudes of objects A and B inside a field of radius $1r_0$ is $p = 0.19$ and 0.29 , respectively. Given the extremely red color of C, and its close distance to galaxy A, we consider C as the most likely host galaxy candidate.

GRB 081204 The field lies at moderate Galactic latitude ($b = -53^\circ$) and is not very crowded with stars. The Galactic reddening is very small, $E(B - V) = 0.03$ mag. The 90% c.l. XRT error circle is the largest in our sample ($r_0 = 5''.3$; Fig. A.1).

We observed the field with VIMOS and ISAAC about 1 year after the burst. Further J -band imaging was performed with SOFI at the NTT nearly 2 years after the event. The field is rich in objects. Within the 90% c.l. error circle lie at least three galaxies (A, B, F; Fig. A.1), which stand together within $5''.0$ and could represent an interacting group. Objects A and B are of similar magnitude ($R_{AB} \sim 23.3$) and size. Object F ($R_{AB} \sim 24.6$) lies very close, north-east of object B. In the VIMOS image it is much fainter than A and B, but in the ISAAC image it stands out by its bright, point-like core ($K_{AB} = 21.5$; Fig. 11). Within the (not so small) photometric errors, it can be classified as an extremely red object. In addition, in the VIMOS image, about $0''.7$ north of F, lies another faint, fuzzy object, but it is too faint for a further analysis. More objects (C–E; G) are seen between $1r_0$ and $2r_0$. The brightest one is a galaxy (C) of similar magnitude and size as objects A and B. Objects D and E ($R_{AB} = 24.2$ and 24.3 , respectively) have a rather blue color of $(R - K)_{AB} < 2.0$ mag and < 0.0 mag, respectively. Object D is not elongated, E is only visible in the VIMOS image, while G is blended with a bright star. Given their faintness it is difficult to decide about their nature. In the ISAAC image, at least G seems to be surrounded by a faint halo, possibly indicating that this is a galaxy.

Deep follow-up observations of the field were also performed with GROND, while (unsuccessfully) searching for the afterglow about 10 hr after the burst (Table A.1; Updike et al. 2008a). Objects A and B are detected in $g'r'i'z'$ (A also in H), while C was only seen in $r'i'J$. Galaxy A is blue, its SED is es-

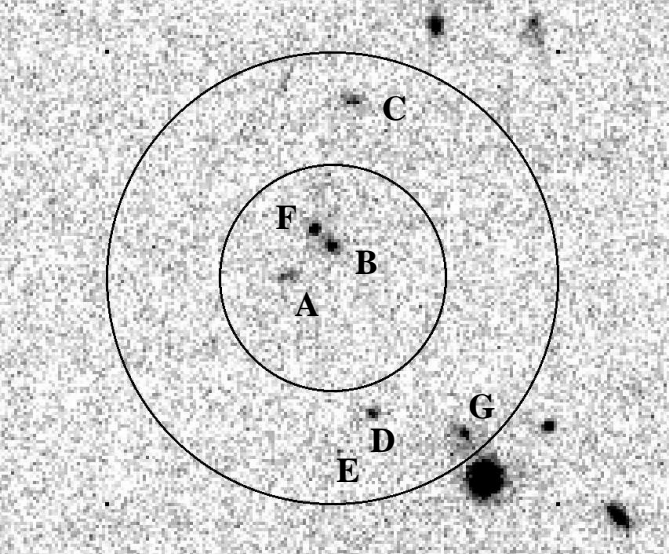


Fig. 11: ISAAC K_s -band image of the field of GRB 081204. Also shown is the 90% c.l. XRT error circle ($r_0 = 5''.3$) as well as a circle of radius $2r_0$. Object F is probably an ERO.

entially flat between R_C and K_s ($(R - K)_{AB} = 0.8 \pm 0.2$ mag), while B is redder ($(R - K)_{AB} = 1.8 \pm 0.1$ mag). Unfortunately, photometric redshift estimates are not very accurate for these galaxies.

The SED of object B shows a jump between the GROND- z' band and the SOFI- J band ($J_{AB} = 22.2$). If this is the 4000Å Balmer break, then the redshift is 1.8 ± 0.3 (Fig. 12). Such a feature is also seen in the SED of galaxy C. Indeed, *Hyperz* finds solutions within the redshift interval $1 < z < 2$ with different sets of extinction laws, galaxy templates, and host extinction values.

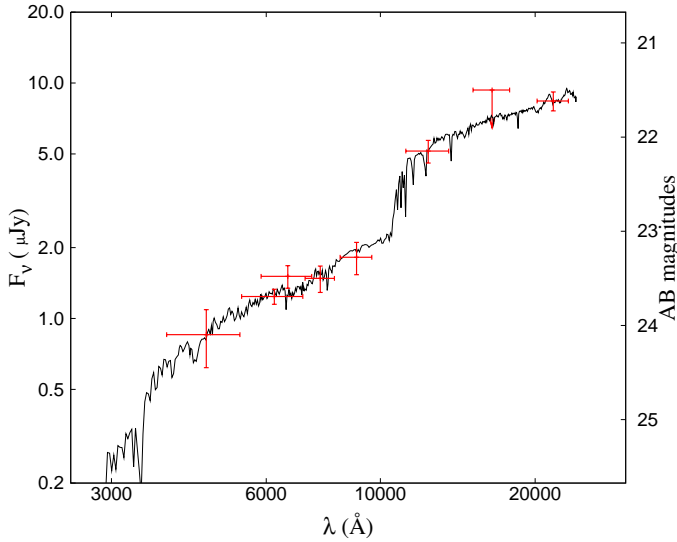


Fig. 12: *Hyperz* best-fit solution of the broad-band SED of object B in the XRT error circle of GRB 081204. The fit suggests a spiral galaxy at a redshift of $z = 1.8 \pm 0.3$ with a moderate intrinsic SMC extinction of $A_{V,host}^{host} = 0.3$ mag ($\chi^2/d.o.f = 0.5$).

Given the connection of long GRBs with young stellar populations, it is appealing to have an interacting group of galax-

ies inside the 90% c.l. error circle. The magnitude-probability criterion gives for objects A and B $p = 0.16$ and $p = 0.19$, respectively, which does not prefer one galaxy over the other. The probability to find a galaxy with the red color of F within an area of radius $1r_0$ is much smaller, however: $p_{ERO} = 0.09$. Therefore, we consider F, which is possibly interacting with B, as the most likely birthplace of GRB 081204.

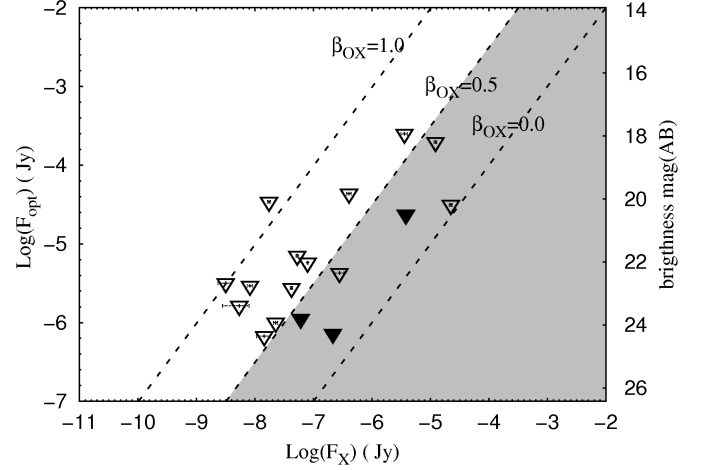


Fig. 13: **Application of the J04 criterion:** Observed upper limits in the R_C band compared to the measured flux density at 1.73 keV (the logarithmic mean of the *Swift*/XRT window, 0.3 – 10 keV) for the 17 bursts in our sample. In those cases where no R_C -band data were available, we used the observed spectral slope β_{OX} to shift the flux density from the native filter to the R band (Table 4). The bursts falling in the gray area fulfill the J04 criterion. The three bursts which can be considered as securely classified dark bursts according to J04 as well as V09 (see Fig. 14) are marked with a filled black triangle (see Sect. 3.4).

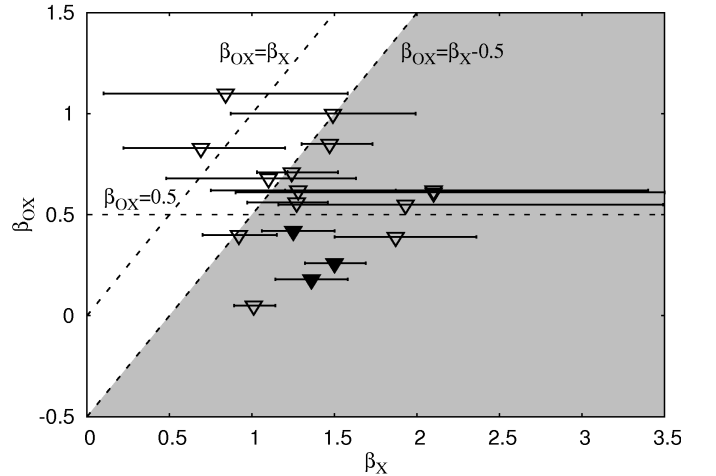


Fig. 14: **Application of the V09 criterion:** Deduced upper limits for the spectral slope β_{OX} as compared to the measured spectral slope of the afterglow in the X-ray band. The same symbols are used as in Fig. 13. The bursts falling in the gray area fulfill the V09 criterion. Here $\beta_{OX} = 0.5$ is highlighted in order to compare with the J04 criterion.

Table 2: Summary of the photometry of all objects found in the XRT error circles based on the VLT observations.

#	GRB	Object	R.A., Dec. (J2000)	R_{AB}	K_{AB}	UL_R	UL_K	XRTpos
2	050922B	–	no candidates	>26.5	>22.8	26.5	22.8	
5	060919	A	18:27:41.78, –51:00:51.0	26.14 ± 0.24	>23.4	26.5	23.4	1
6	060923B	A ^a	15:52:46.49, –30:54:12.3	23.10 ± 0.11	21.76 ± 0.09	26.6	24.3	2
		B ^a	15:52:46.61, –30:54:10.3	21.67 ± 0.02	18.95 ± 0.03	26.6	24.3	2
		C ^a	15:52:46.56, –30:54:14.6	24.49 ± 0.04	22.87 ± 0.15	26.6	24.3	1
		D ^a	15:52:46.63, –30:54:16.4	25.74 ± 0.12	21.63 ± 0.06	26.6	24.3	2
		E ^a	15:52:46.66, –30:54:12.9	blended with A	blended with A	26.6	24.3	1
7	061102	A	09:53:37.93, –17:01:22.7	24.10 ± 0.06	>22.8	26.9	22.8	2
		B	09:53:37.89, –17:01:30.8	23.96 ± 0.06	>22.8	26.9	22.8	2
8	070429A	A	19:50:48.78, –32:24:13.6	25.01 ± 0.20	22.57 ± 0.25	26.5	23.8	3
		B ^a	19:50:48.78, –32:24:18.1	24.14 ± 0.09	22.39 ± 0.21	26.5	23.8	1
		C ^a	19:50:48.90, –32:24:17.4	24.32 ± 0.08	21.89 ± 0.14	26.5	23.8	1
		D	19:50:49.10, –32:24:17.3	>26.5	23.01 ± 0.40	26.5	23.8	2
9	070517A	A	18:30:29.08, –62:17:53.0	25.39 ± 0.21	>23.4	26.6	23.4	1
10	080207	A	13:50:03.03, +07:30:09.3	25.15 ± 0.17	23.02 ± 0.39	26.9	23.6	2
		B	13:50:02.97, +07:30:07.2	26.49 ± 0.37	21.77 ± 0.14	26.9	23.6	1
11	080218B	A	11:51:49.69, –53:05:49.1	26.23 ± 0.13	21.74 ± 0.10	27.3	24.0	1
		B	11:51:50.00, –53:05:47.4	24.62 ± 0.04	22.74 ± 0.24	27.3	24.0	3
12	080602	A	01:16:42.15, –09:13:55.0	22.95 ± 0.02	22.55 ± 0.05	26.9	23.5	1
		B	01:16:42.12, –09:13:57.5	24.00 ± 0.06	>23.5	26.9	23.5	2
		C	01:16:42.14, –09:13:53.4	>26.9	22.49 ± 0.14	26.9	23.5	2
13	080727A	–	no candidates	>26.3	>23.0	26.3	23.0	
14	080915A	A	01:11:47.80, –76:01:13.9	21.63 ± 0.01	20.42 ± 0.02	26.3	23.4	1
		B	01:11:45.27, –76:01:10.4	21.28 ± 0.01	19.19 ± 0.01	26.3	23.4	3
		C ^a	01:11:47.47, –76:01:10.0	24.71 ± 0.07	>23.4	26.3	23.4	1
		D ^a	01:11:46.98, –76:01:09.5	24.57 ± 0.08	>23.4	26.3	23.4	2
		E ^a	01:11:47.16, –76:01:15.1	25.44 ± 0.15	>23.4	26.3	23.4	1
15	081012	A	02:00:48.18, –17:38:15.2	25.16 ± 0.17	>23.9	26.7	23.9	2
16	081105	A	00:15:48.42, +03:28:11.6	23.73 ± 0.08	22.78 ± 0.18	26.1	24.5	1
		B	00:15:48.30, +03:28:13.8	24.34 ± 0.13	22.13 ± 0.14	26.1	24.5	1
		C	00:15:48.46, +03:28:10.7	>25.3	21.74 ± 0.13	26.1	24.5	1
17	081204	A ^b	23:19:09.39, –60:13:31.5	23.21 ± 0.04	22.37 ± 0.16	26.4	24.3	1
		B ^a	23:19:09.13, –60:13:30.2	23.46 ± 0.04	21.59 ± 0.08	26.4	24.3	1
		C	23:19:08.99, –60:13:23.4	23.16 ± 0.07	22.06 ± 0.11	26.4	24.3	2
		D	23:19:08.89, –60:13:37.6	24.19 ± 0.10	22.16 ± 0.15	26.4	24.3	2
		E	23:19:09.10, –60:13:39.4	24.32 ± 0.12	>24.3	26.4	24.3	2
		F ^a	23:19:09.24, –60:13:29.4	24.65 ± 0.50	21.53 ± 0.07	26.4	24.3	1
		G	23:19:08.30, –60:13:39.0	blended with a star	21.57 ± 0.15	26.4	24.3	2

Notes: Column: (2) GRB 050717, GRB 060211A, and GRB 060805A are the only bursts in our sample for which we do not have VLT data (see Table 3). (3) Objects identified in the XRT error circles (see Sect. 3.3). (5) Observed magnitudes. UL stands for the 3σ upper limit. The last column defines the distance of the object from the center of the 90% XRT error circle of radius r_0 (see Table 1). A value n means that the source lies within $[(n-1)r_0, nr_0]$. *Special notes about the photometry:* All magnitudes are based on (2× FWHM) aperture photometry, except for those cases where the object was affected by near-by objects. In the latter case we used either (a) PSF photometry or (b) 1× FWHM aperture photometry. In particular, we gave preference to the latter in the case of elongated objects.

Table 3: Summary of the photometry of all objects found in the XRT error circles based on observations with GROND.

#	GRB	Obj.	R.A., Dec. (J2000)	g'_{AB}	r'_{AB}	i'_{AB}	z'_{AB}	J_{AB}	H_{AB}	K_{AB}	XRTpos
1	050717	A	14:17:24.56, −50:31:58.7	> 25.4	23.65(10)	23.01(11)	23.40(30)	>22.6	>21.9	>21.1	2
		B ^b	14:17:24.58, −50:32:01.6	> 25.4	24.50(40)	23.50(40)	22.80(30)	>22.6	>21.9	>21.1	1
3	060211A	A	03:53:32.66, +21:29:19.8	> 25.2	24.51(20)	> 24.8	> 24.4	>23.4	>21.6	>21.6	1
		B	03:53:32.43, +21:29:16.3	23.60(08)	23.09(06)	22.76(09)	23.31(10)	<23.1	>21.6	21.50(20)	3
		C	03:53:32.57, +21:29:18.0	> 25.2	> 24.9	> 24.8	> 24.4	23.1(30)	>21.6	>21.6	1
		D	03:53:32.69, +21:29:20.90	> 25.2	> 24.9	> 24.8	> 24.4	23.4(40)	>21.6	>21.6	2
4	060805A	A	14:43:43.49, +12:35:12.5	>25.5	25.4(40)	> 24.6	> 24.2	>22.9	>21.8	>21.1	1
		B	14:43:43.39, +12:35:10.1	23.42(16)	23.68(12)	> 24.6	> 24.2	>22.9	>21.8	>21.1	2
10	080207	A-B	see Table 2	>25.4	>24.9	>23.9	>23.8	>22.0	>20.8	>20.1	1,2
11	080218B	A	see Table 2	>25.5	>24.9	>24.2	>24.1	>22.8	>21.4	>21.2	1
		B	see Table 2	25.10(30)	24.30(30)	—	23.27(10)	>22.8	>21.4	>21.2	3
12	080602	A	see Table 2	22.96(10)	22.93(08)	22.86(13)	22.60(14)	>21.4	>21.0	>20.6	1
		B	see Table 2	>25.3	23.73(12)	23.90(29)	22.97(17)	>21.4	>21.0	>20.6	2
		C	see Table 2	>25.3	>25.5	>24.9	>24.6	>21.4	>21.0	>20.6	2
14	080915A	A	see Table 2	22.05(10)	21.27(10)	21.21(10)	20.80(10)	20.53(02)	20.37(03)	20.39(15)	1
		B	see Table 2	23.30(30)	21.14(05)	20.88(06)	20.28(12)	19.74(06)	19.33(06)	19.00(08)	3
		C-E	see Table 2	>24.0	>24.3	>24.1	>23.9	>22.1	>21.3	>21.3	1,2
15	081012	A	see Table 2	>23.8	>23.8	>23.4	>23.2	>21.8	>21.3	>21.0	2
16	081105	A-C	see Table 2	>24.0	>23.9	>23.3	>22.9	>21.4	>20.7	>20.3	1
17	081204	A ^b	see Table 2	23.69(10)	23.74(08)	23.25(11)	23.09(15)	22.50(16)	>21.5	>20.9	1
		B ^b	see Table 2	24.18(30)	23.74(08)	23.53(14)	23.29(17)	22.15(15)	>21.5	>20.9	1
		C	see Table 2	>25.0	23.96(17)	23.62(28)	>24.0	22.55(19)	>21.5	>20.9	2
		D-G	see Table 2	>25.0	>25.0	>24.7	>24.0	>22.0	>21.5	>20.9	1,2

Notes. Columns (4-10): Observed magnitudes. Magnitude errors are given in units of 10 mmag. In case of GRB 060211A we report the NEWFIRM J and K_s -band results. In the case of GRB 081204 we report the NTT/SOFI J -band results. For GRB 080218B the i' -band data are affected by a ghost image from a bright star. Upper limits are 3σ . *Special notes about the photometry:* (b) see Table 2.

3.4. Adding X-ray data: which bursts are truly optically dark?

According to Jakobsson et al. (2004) (hereafter J04), a GRB with a detected X-ray afterglow is considered dark if the spectral slope between the optical and the X-ray regimes obey the relation $\beta_{OX} < 0.5$, while according to van der Horst et al. (2009) (hereafter V09) a burst is optically dark if $\beta_{OX} < \beta_X - 0.5$ (see also Rol et al. 2005). Both definitions are suited to find additional dimming of the optical flux as compared to the observed X-ray flux, assuming standard afterglow theory (eg., Sari et al. 1998; Rossi et al. 2011).

In order to determine β_X and β_{OX} , we used the data from the *Swift*/XRT GRB light curve and spectrum repository (Evans et al. 2007, 2009). Typically, the optical upper limits and X-ray data were not obtained at the same time. Therefore, we fit the X-ray light curves in order to interpolate the X-ray flux contemporaneous to the corresponding optical/NIR upper limits. Please note that the collected upper limits come from GCNs and often these values are not well calibrated or even contain systematic errors. In the case of observations performed with GROND or where we were able to collect the original data there are no calibration issues (GRBs 070429A, 070517A, 080207, 080218B, 080727A, 080915A, 081012, 081105, 081204). In the other cases one can introduce a systematic error, for example 0.5 mags. This translates in a ~ 0.07 systematic error in the value for the upper limit of β_{OX} and in ~ 0.5 in the value of the extrapolated upper limit in the R_C band. Therefore, one has to keep in mind this effect in the following. Given that this is difficult to estimate, it will not be considered in our calculation. Likely, as we will show, this systematic will not affect the burst classified as

dark GRBs. Given that bluer filters are more affected by Lyman drop-out and uncertainties in the extinction, we gave preference to the upper limits obtained in red filters. However often the redder filter resulted to be the UVOT v -band, while we used to shift in the R_C band in order to compare with other afterglow light-curves (Fig. 1) and for visualize the J04 criterion in a common picture (Fig. 13). While shifting from redder to bluer filter can only result in overestimating the optical flux and therefore β_{OX} , shifting from v -band to the R_C -band can underestimate the flux and the β_{OX} upper limit. This is true especially in case the Lyman drop-out falls between v and R_C -bands. However, note that this fact does not affect the J04 or V09 criterion used here, because only the native filters were used to compute β_{OX} upper limits, and the extrapolation to a common R_C -band were used only for better visualizing the results. For the X-rays, we used the flux density at 1.73 keV (corrected for Galactic absorption), which is the logarithmic mean of the *Swift*/XRT window (0.3 – 10 keV). Where the X-ray data are concerned, we gave priority to those time intervals where the light curves were smoothly decaying (which differ from burst to burst) and during which β_X was constant (within the errors). If possible, we used only optical upper limits that were taken at times reasonably separated from the prompt GRB phase. Among all computed values, we chose those that implied the lowest β_{OX} values.

Table 4 summarizes our results. Here $\Delta = \beta_X - \beta_{OX} - 0.5$. To be conservative, we used its minimum value Δ_{min} , based on the 90% c.l. error of β_X . If $\Delta_{min} > 0$, a burst is classified as dark according to V09. Five events, namely GRBs 050922B, 070429A, 080207, 080218B, and 080602, are dark according to both def-

initions, while GRB 050717 is dark according to J04 only and GRBs 080915A and 081204 are dark only according to V09 (Figs. 13, 14). Following the above discussion, we consider a GRB dark if it fulfills both the criterion of J04 and V09.

We note that at the time when the optical upper limits were obtained some shortcomings could limit the validity of this approach: (1) an X-ray light curve that is rather flat than decaying might point to an additional X-ray component, while the aforementioned procedure assumes a single radiation component (this affects GRB 080602), (2) a substantial time gap in the X-ray data base (GRB 050922B), (3) an evolving X-ray spectral slope (GRB 050717), and (4) a large measurement error (> 1) of the X-ray spectral slope (GRB 080915A, 081105, and 081204). Taking all this into account, only three events in our sample can be securely classified as dark bursts (GRBs 070429A, 080207A, 080218B). All other bursts, except GRB 070517A, can still be truly dark bursts but the available data are not sufficient to claim this with certainty.

4. Discussion

In the following, we first classify the host galaxy candidates we have found. Then, we focus on the implications of our findings of ERO galaxies for the interpretation of the optical dimness of the afterglows in our sample.

4.1. Magnitude-probability candidates

These are host candidates defined by the probability p to randomly find a galaxy of the given R -band magnitude inside an area with the size of the corresponding XRT error circle (Sect. 3.2; Table 5). We arbitrarily required $p \leq 0.1$ (within the 1σ error). The corresponding host galaxy candidates are: GRB 050717, objects A and B; GRB 060211A, objects A and B; GRB 060805A, objects A and B; GRB 060923B, objects A and C; GRB 070429A, objects B and C; GRB 070517A, object A; GRB 080207, object B; GRB 080602, object A; GRB 080915A, object C. Note that in the case of GRB 070429A two galaxies have $p \leq 0.1$, and our VLT data reveal that they could constitute a tightly bound pair. Note also that the optical afterglow of GRB 070517A has been identified in the present paper (Sect. 3.3) and in this case p gives the corresponding probability to find the galaxy labeled A (Fig. A.1) at the given angular distance from the afterglow position.

The other cases in our sample have $p > 0.1$, either because the detected galaxies are too faint, the XRT error circles are too big, or a mixture of both. Also, if more than one galaxy is found inside an XRT error circle, this criterion does not often prefer one candidate over the other, as the differences in the corresponding p -values are not sufficiently large (e.g., GRB 050717 and GRB 061102; Table 5). This situation changes, however, if we consider number counts of extremely red objects.

4.2. Extremely red objects as candidates

Long bursts trace the birth places of the most massive stars (e.g., Fruchter et al. 2006), which leads to the expectation that a certain percentage of hosts of long bursts are dust-enshrouded, starburst galaxies. Among them, the most extreme cases are classified as EROs. So far, there is only a small number of hosts known which enter this category: GRB 020127 (Berger et al. 2007), GRB 030115 (Levan et al. 2006; Dullighan et al. 2004), GRB 070521 (Perley et al. 2009), GRB 080207 (Hunt et al. 2011;

Svensson et al. 2011), GRB 080325 (Hashimoto et al. 2010) as well as GRB 080607 (Chen et al. 2010, 2011; Perley et al. 2011).

In our sample, seven objects fall (within their 1σ magnitude error) into this category (Table 5). These are: GRB 060923B, object D with $(R - K)_{AB} = 3.82 \pm 0.13$ mag; GRB 070429A, object D with > 3.5 mag (within the 1σ error in K_s); GRB 080207, object B with 4.66 ± 0.40 mag; GRB 080218B, object A with 4.15 ± 0.16 mag; GRB 080602, object C with > 4.3 mag; GRB 081105, object C with > 3.5 mag; GRB 081204, object F with 3.1 ± 0.5 mag. Three of them lie within the corresponding 90% c.l. XRT error circle (GRB 080207, 080218B, and 081204), one object lies at $1r_0$ (GRB 081105), the other three objects lie within less than $1.5r_0$. All objects have very small p -values based on number counts of EROs on the sky (Gonzalez-Perez et al. 2009).

4.3. Lyman-dropout candidates

For two of the 17 bursts investigated here (GRBs 050922B and 080727A) we could not find any galaxy inside $2r_0$, where r_0 is the corresponding 90% c.l. XRT error circle radius. Therefore, we consider the optical afterglows of these events as Lyman drop-out candidates. Though we cannot rule out very faint hosts at $z \lesssim 5$.

An additional, but weaker Lyman drop-out candidate, is the optical afterglow of GRB 081012. Here we find only one galaxy between $1r_0$ and $2r_0$. As we have noted in Sect. 3.3, if we consider this as the host, then the offset of the afterglow from the center of this galaxy would be quite large. Therefore, an alternative interpretation would be that the host is not detected in our deep VLT images, i.e. it could be Lyman dropped out.

In two other cases a galaxy is found not closer than $1r_0$ from the center of the corresponding error circle (GRBs 060923B and 061102), but the galaxy's outer parts extend to within the 90% c.l. XRT error circle. In other words, here the afterglow could have been placed well inside $1r_0$. Therefore, we do not consider the optical afterglows of these two bursts as Lyman drop-out candidates.

Finally, among the seven ERO galaxies discovered in our sample, four have been detected in R , i.e. they are not Lyman dropped out. On the other hand, those three ERO galaxies with no R -band detection could lie at higher redshifts (GRB070429A/object D, GRBs 080602/object C and 081105/object C).

We conclude, in our sample we have up to six Lyman drop-out candidates ($\sim 30\%$), in all other cases such an interpretation is not required. Given the low-number statistics, we consider this as being in qualitative agreement with Perley et al. (2009), who found that in their sample of optically non-detected afterglows at most 14% are at a redshift $z > 5$.

4.4. Interacting pairs of galaxies as candidates

Since long bursts are related to star formation, their host galaxies could be interacting, morphologically disturbed galaxies, where a starburst was triggered by galaxy-galaxy-interaction (e.g., Fruchter et al. 1999). In our images, we find four such potential cases where at least one partner lies inside the 90% c.l. XRT error circle. These are GRB 070429A, objects B and C (R_C band; Fig. A.1); GRB 080602, objects A and C (K_s band; Fig. 7); GRB 080915A, objects C and D (R_C and K_s band; Figs. A.1, 9) as well as GRB 081204, objects B and F (R_C and K_s band;

Table 4: Summary of the darkness properties of our sample.

# (1)	GRB (2)	Time (s) (3)	UL (4)	Filter (5)	UL _R (6)	Ref. (7)	β_{OX} (8)	β_X (9)	Δ_{min} (10)	Comments (11)
1	050717	420	19.0	ν	18.2	GCN 3638	< 0.40	$0.92^{+0.23}_{-0.22}$	-0.20	a; b
2	050922B	49000	22.5	r'	22.3	GCN 4025	< 0.39	$1.87^{+0.49}_{-0.37}$	0.61	c
3	060211A	19980	22.0	R_C	21.8	GCN 4927	< 0.71	$1.24^{+0.23}_{-0.21}$	-0.18	–
4	060805A	63000	22.9	r'	22.7	GCN 5406	< 1.00	$1.49^{+0.50}_{-0.62}$	-0.63	–
5	060919	918	20.2	ν	19.8	GCN 5580	< 0.68	$1.10^{+0.53}_{-0.62}$	-0.70	a
6	060923B	295	18.5	ν	17.9	GCN 5603	< 0.62	$1.28^{+0.59}_{-0.53}$	-0.37	b
7	061102	1480	20.5	ν	20.1	GCN 5784	< 1.10	$0.84^{+0.74}_{-0.74}$	-1.50	d
8	070429A	44064	24.0	R_C	23.8	GCN 6371	< 0.42	$1.25^{+0.25}_{-0.19}$	0.14	•; g
9	070517A	57600	24.5	i'	24.3	GCN 6420	< 0.56	$1.27^{+0.19}_{-0.30}$	-0.09	f
10	080207	5364	20.3	R_C	20.5	GCN 7333	< 0.26	$1.50^{+0.19}_{-0.18}$	0.56	•
11	080218B	11520	24.7	r'	24.3	Table A.1	< 0.18	$1.36^{+0.22}_{-0.22}$	0.46	•
12	080602	504	20.3	ν	20.2	GCN Rep. 145.1	< 0.05	$1.01^{+0.13}_{-0.12}$	0.34	e
13	080727A	2268	19.8	K	22.8	GCN 8048	< 0.85	$1.47^{+0.26}_{-0.17}$	-0.05	–
14	080915A	6840	22.1	I_C	22.1	GCN 8248	< 0.62	$2.10^{+1.30}_{-0.90}$	0.08	d
15	081012	69660	23.5	r'	23.4	Table A.1	< 0.83	$0.69^{+0.51}_{-0.47}$	-1.11	–
16	081105	46224	23.0	r'	22.8	Table A.1	< 0.61	$2.10^{+1.70}_{-1.20}$	-0.21	d
17	081204	34560	24.1	r'	23.9	Table A.1	< 0.55	$1.93^{+1.56}_{-0.77}$	0.11	d

Notes: *Columns:* (3 to 5) Time after the burst and reported upper limits (UL) of the afterglow (observed magnitudes); r' -band magnitudes are given in the AB system, all others in the Vega/UVOT system. (6) Deduced UL in the R_C band (AB system) after correcting for Galactic extinction and after shifting from the native filter wavelength (column 5) to the R_C band using the upper limit on β_{OX} . (8) If $\beta_{\text{OX}} < 0.5$ then a burst is dark according to J04. (10) The minimum value (based on the 90% confidence error of β_X) of the quantity $\Delta = \beta_X - \beta_{\text{OX}} - 0.5$. If $\Delta_{\text{min}} > 0$ then a burst is dark according to V09. (11) (a) During the time of the observed UL the SED in the X-ray band is not constant. (b) The observed UL lies close to the end of the prompt GRB phase. (c) No X-ray data exist at the time when the UL was obtained. (d) Very faint X-ray flux; no well-defined X-ray light curve. (e) Flat X-ray light curve during the time when the UL was obtained. (f) The optical afterglow was detected; see Sect. 3.3. (g) No UL is reported in the corresponding GCN (Price 2007). We used $R_C = 24.0$ based on the original data which are available in the Gemini archive. A bullet (•) indicates that the burst is truly dark according to J04 and V09 (Sect. 3.4). *Column (7; references):* 1. Blustin et al. (2005); 2. Guziy et al. (2005); 3. Sharapov et al. (2006); 4. Rol & Page (2006); 5. Breeveld & Guidorzi (2006); 6. Holland & Cucchiara (2006); 7. Holland (2006); 8. Price (2007); 9. Fox et al. (2007); 10. Cucchiara & Ukwatta (2008); 11. Andreev et al. (2008); 13. Beardmore et al. (2008e); 14. Levan & Wiersema (2008); 15. Rossi et al. (2008c)

Figs. A.1, 11). Also object B in the field of GRB 061102 looks morphologically disturbed (Fig. A.1) but no other galaxy very close to it is seen in our images.

There are no statistics at hand that could provide chance probability values for finding an interacting pair of galaxies in a randomly chosen area on the sky. Nevertheless, we conclude that the search for an interacting pair could be a good selection criterion to find GRB host galaxy candidates (see also Wainwright et al. 2007).

4.5. Normal candidates

The fields of five bursts (GRBs 050717, 060211A, 060805A, 060919, and 081012) stand out in our sample. In these cases galaxy candidates are seen in the corresponding XRT error circle, at least within $2r_0$, but no EROs are found, nor is there evidence of an interacting pair. We must conclude that if one of these is the host, then it is a normal galaxy, i.e., typical for host galaxies of not extinguished GRBs. This is in agreement with Perley et al. (2009), who found that in their sample most dark burst host galaxies are normal GRBHs, phenomenologically not different from the hosts of bursts with optically detected afterglows.

A special case is GRB 070517A, where we could identify the optical afterglow based on the early observations by Fox et al. (2007). Here only one object is found within $1r_0$, but this object is offset from the position of the optical afterglow by 1.6 arcsec.

A redshift $z \lesssim 0.5$ is required in order to avoid a projected offset in kpc which is rather large compared to the observed mean of the GRB offset distribution (Bloom et al. 2002). This redshift then further implies a subluminal galaxy (see Sect. 4.6), but otherwise no strong constraints on its properties can be set.

4.6. Redshift estimates

No precise redshifts are known for the galaxies we have found in the XRT error circles. In the case of GRBs 080602 and 081204 the redshift is surely below 3.5 due to the detection of the objects in the GROND g' band but no further constraints can be set. Therefore, we use two approaches to obtain redshift estimates.

First, in Table A.3 we provide estimated redshifts by assuming the galaxies have absolute magnitudes of $M_R = -22, -20$, and -18 , respectively. The first value is about 1 mag below the most luminous galaxies found in the Las Campanas redshift survey ($M_R = -23$; Lin et al. 1996). The middle value is approximately the characteristic M^* of the corresponding Schechter r -band luminosity function. The third value roughly corresponds to the absolute magnitude of the Large Magellanic Cloud. By adopting a power-law spectrum for the SED of the form $F_\nu \propto \nu^{-\beta}$, we then calculate the corresponding redshift for two different spectral slopes ($\beta = 0.0$ and 1.0).⁵ If the deduced

⁵ Thereby, the absolute R -band magnitude is given by $M_R = m_R - \mu - k$, where μ is the distance modulus and k is the cosmological k -correction, $k = -2.5(1 - \beta) \log(1 + z)$.

Table 5: Summary of the properties of the objects found in the XRT error circles.

#	GRB	Object	<i>R</i> -band size	<i>K_s</i> -band size	Comment	$(R - K)_{AB}$	$(R - K)_{Vega}$	XRTpos	<i>p</i>	<i>p_{ERO}</i>
1	050717	●A	2.1 × 3.9	not visible	G	< 1.98	< 3.61	2	0.05±0.01	
		●B	1.2 × 1.3	not visible		< 2.83	< 4.46	1	0.03±0.01	
2	050922B	no candidates								
3	060211A	●A	1.1 × 1.2	not visible	G	< 2.53	< 4.16	1	0.03±0.01	
		●B	3.8 × 2.2	3 sources	G	< 1.21	2.84 ± 0.21	3	0.08±0.01	
		●C	only in <i>J</i>	—	G	—	—	1	—	
		●D	only in <i>J</i>	—	—	—	—	1	—	
4	060805A	●A	1.5 × 1.1	not visible	G	< 4.3	< 5.9	1	0.06±0.01	
		●B	2.7 × 1.3	not visible	G	< 2.5	< 4.1	2	0.09±0.01	
5	060919	●A	1.5 × 1.4	not visible		< 2.60	< 4.23	1	0.15±0.03	
6	060923B	A	2.1 × 2.2	2.2 × 1.8	G	1.05	2.68 ± 0.14	2	0.06±0.01	
		B	2.0 × 2.0	1.9 × 1.9	S	2.43	4.06 ± 0.04	2	—	
		C	1.1 × 1.0	0.8 × 0.8		1.33	2.96 ± 0.16	1	0.04±0.01	
		●D	1.3 × 1.3	0.8 × 0.8	G	3.82	5.45 ± 0.13	2	0.37±0.03	0.04±0.01
		E	blended with A	blended with A				1	—	
7	061102	●A	2.5 × 1.5	not visible	G	< 1.22	< 2.85	2	0.34±0.01	
		●B	1.8 × 1.9	not visible	G	< 1.08	< 2.71	2	0.31±0.01	
8	070429A	A	3.8 × 1.4	1.9 × 1.1	G	2.10	3.73 ± 0.32	3	0.54±0.05	
		●B	2.8 × 1.4	blended with C	G	1.41	3.04 ± 0.23	1	0.04±0.01	
		●C	1.7 × 1.5	1.5 × 1.0	G	2.09	3.72 ± 0.16	1	0.05±0.01	
		●D	not visible	1.6 × 1.0	G	> 3.1	> 4.7	2	—	0.07±0.01
9	070517A	●A	1.6 × 1.3	not visible	G	< 1.69	< 3.32	1	0.07±0.02	
10	080207	A	2.4 × 1.3	not visible	G	2.08	3.71 ± 0.43	2	0.20±0.02	
		●B	2.1 × 1.1	1.6 × 0.9	G	4.66	6.29 ± 0.40	1	0.14±0.04	0.01±0.01
11	080218B	●A	2.5 × 1.1	1.4 × 0.7	G	4.15	5.78 ± 0.16	1	0.12±0.01	0.01
		B	1.6 × 1.5	0.8 × 0.8		1.54	3.17 ± 0.24	3	0.28±0.01	
12	080602	●A	2.6 × 2.0	1.2 × 0.8	G	0.34	1.97 ± 0.05	1	0.01±0.01	
		B	2.0 × 1.8	not visible	G	< 0.44	< 2.07	2	0.13±0.01	
		●C	not visible	1.2 × 0.8	G	> 4.35	> 5.98	2	—	0.04±0.01
13	080727A	no candidates								
14	080915A	A	3.5 × 3.5	1.2 × 1.2	S	1.11	2.74 ± 0.02	1	—	
		B	5.6 × 4.5	3.4 × 1.8	G	1.99	3.62 ± 0.01	3	0.16±0.01	
		●C	1.2 × 1.2	not visible	G	< -0.29	< 1.34	1	0.08±0.01	
		●D	1.2 × 1.2	not visible	G	< 0.03	< 1.66	2	0.35±0.01	
		E	1.5 × 1.5	not visible		< 1.94	< 3.57	1	0.13±0.01	
15	081012	●A	1.8 × 1.5	not visible	G	< 1.21	< 2.84	2	0.31±0.03	
16	081105	A	1.2 × 1.2	1.0 × 1.0	G	0.89	3.56 ± 0.15	1	0.19±0.01	
		B	1.1 × 1.1	0.8 × 0.8		2.15	3.78 ± 0.19	1	0.29±0.02	
		●C	not visible	0.8 × 0.5	G	> 3.50	> 5.13	1	—	0.08±0.01
17	081204	A	2.1 × 1.4	0.9 × 0.5	G	0.79	1.61 ± 0.16	1	0.16±0.01	
		B	2.7 × 1.4	1.1 × 0.8	G	1.82	2.74 ± 0.09	1	0.19±0.01	
		C	2.2 × 1.7	0.9 × 0.6	G	1.05	2.58 ± 0.13	2	0.49±0.02	
		D	1.2 × 1.2	0.5 × 0.5		1.98	< 1.46	2	0.78±0.03	
		E	1.2 × 1.2	not visible		< -0.04	< 1.59	2	0.81±0.03	
		●F	~ 1	0.6 × 0.6	G	3.1	4.7 ± 0.50	1	0.67±0.11	0.09±0.01
		G	blended with a star	1.5 × 1.5		—	—	2	—	

Notes: (1) A bullet (●) in column #2 indicates the most likely GRB host candidate. If more than one candidate is marked then we cannot determine which is the best. For details about the selection, see Sect. 3.3. GRBs that are truly dark according to J04 and V09 are highlighted in boldface. (2) Angular sizes are given in units of arcsec. (3) Magnitude errors in $(R - K)_{AB}$ are identical to the corresponding errors for $(R - K)_{Vega}$. Colors are corrected for Galactic extinction. (4) The last two columns gives the chance probability *p* of finding a galaxy of the corresponding extinction-corrected (Vega) *R*-band magnitude on the sky in a region with the size of the corresponding X-ray error circle with a radius $r = \text{XRTpos} \times r_0$ (Eq. 1). Thereby, the first column refers to number counts of galaxies of all kinds. If the object is for sure a star, then no value is given. The second column refers to number counts of EROs only (see Sect. 4.8). (5) Comment “G” stands for galaxy, “S” for star; if no letter is given then we could not determine if this is a star or a galaxy. (6) In case of GRB 070517A, the probability *p* is based on the distance between the afterglow and galaxy A, (1''6; Sect. 3.3). GRB 070429A/object D and GRB 081204/object F are EROs within the large 1σ photometric error.

redshift is larger than 5, Lyman dropout in the R -band could have affected the apparent magnitudes and no values for z are given. We find that most galaxies less luminous than the Milky Way Galaxy probably lie at redshifts smaller than $z = 2$.

As a second approach we used the $E_{\text{peak}}-E_{\text{iso}}$ correlation for long GRBs (Amati 2006) by analyzing the *Swift*/BAT or Konus-Wind spectrum. Unfortunately, for the majority of the bursts the required spectral information for this analysis is not available. Only in five cases did we obtain results, though they are not very constraining (Table A.4). In the case of GRB 080207 and GRB 080602 the $E_{\text{peak}}-E_{\text{iso}}$ relation constrains the redshift to $z > 0.9$ (2σ) and $z > 1$ (2σ), respectively, in agreement with the photometric redshifts found for GRB 080207 ($z \sim 2.2$; Sect. 3.3) and GRB 080602 ($z \sim 1.4$; Sect. 3.3).

4.7. Host galaxy candidates of truly dark bursts

Fynbo et al. (2009) shows that at least 39% of optically dim GRB afterglows are dark according to the J04 criterion. In our sample GRBs 070429A, 080207, and 080218B are truly optically dark (Sect. 3.4) and also belong to our small subsample of bursts with extremely red host galaxy candidates (Sect. 4.2). This strongly supports the idea that global dust extinction in their host galaxies was responsible for dimming the afterglow in the optical bands. This holds especially for GRB 080207, for which we can be sure that the host galaxy is object B, thanks to the precise localization of its X-ray afterglow by *Chandra*.

In the case of GRB 080218B, a host galaxy candidate is visible in the R_C -band, constraining its redshift to $z \lesssim 5$. For this event, Greiner et al. (2011) find that different pairs of (z, A_V) solutions can explain the non-detection of the optical/NIR afterglow by GROND. For example, for a redshift of 3.5 a host extinction of $A_V^{\text{host}} = 1.5$ mag is required. A lower redshift would increase the deduced amount of host extinction even more; however studies of *optically detected* GRB afterglows (e.g., Kann et al. 2010) show that such extinction values would be very high compared to the norm. Nevertheless, host galaxies having low extinction may be linked with optical detection of GRB afterglows; more statistics are needed to establish how common high values of extinction really are.

Another ERO, the host of GRB 070429A not detected in R_C , lies just on the border of the 90% c.l. XRT error circle. It is a less compelling candidate than either GRB 080207 or GRB 080218B because it is also very faint in K_s , with a correspondingly large photometric error of 0.4 mag. Also, in this case there are two more galaxies within the 90% c.l. error circle. Their $(R - K)$ colors are not particularly red, however. If the very red galaxy would be confirmed as an ERO, then our study points to a strong link between optically dim GRB afterglows and ERO galaxies.

4.8. EROs as an important subpopulation of GRB host galaxies

The seven EROs we have identified have magnitudes between $K_{\text{AB}} = 21.6$ and 23.0 , i.e. $K_{\text{Vega}} = 19.8$ to 21.1 (Table 2). For these K -band magnitudes the number density of EROs on the sky is in the order of 1 per 1000 arcsec² (Gonzalez-Perez et al. 2009; Hempel et al. 2011; Kim et al. 2011).⁶ Our findings then imply an overdensity of EROs in the XRT error circles we have studied here. Four of the seven EROs we have found lie inside their corresponding 90% c.l. XRT error circle. In the remaining three

cases (GRBs 060923B, 070429A and 080602) the ERO lies just close to the border of the 90% c.l. error circle (see Sect. 3.3).

Because long GRBs are thought to trace the formation of massive stars (passively evolving ellipticals cannot be their hosts), the immediate conclusion that can be drawn from our study is that bursts with optically non-detected afterglows (but with rapid and deep follow-up observations) trace a subpopulation of massive galaxies undergoing violent star formation. This holds for dark bursts in particular: all three bursts investigated here which belong to this class have an ERO within or close to their 90% c.l. XRT error circle (GRBs 070429A, 080207 and 080218B). If we consider as dark all GRBs that follow the J04 or V09 criterion (but keeping in mind that this now includes events where the X-ray data are not so easily interpreted, see Sect. 3.4), then we have eight such GRBs in our sample (Table 4); five of them have an ERO within or close to their 90% c.l. error circle (in addition these are GRBs 080602 and 081204). It should be stressed that, in principle, all GRBs studied here except GRB 070517A (for which we identified the afterglow; Sect. 3.3) could be truly dark bursts according to the criterion from J04 and V09; we just do not have sufficiently deep optical limits to be certain.

Several previous studies have already targeted GRBHs (e.g., Le Floc'h et al. 2003; Christensen et al. 2004; Fruchter et al. 2006; Ovaldsen et al. 2007; Svensson et al. 2010 and SBG09). They focused on the low-redshift regime (up to $z \sim 1.5$) and showed that most hosts are subluminal ($L < L^*$), blue, of low metallicity and with a moderate star formation rate ($\sim 1 - 10 M_{\odot} \text{ yr}^{-1}$). However, our results suggest that an infrared-bright subpopulation of very dusty GRBHs could exist, which stands out from the main GRB host galaxy population.

Redshift measurements for the EROs we have identified here are missing in most cases up to now. However, for the ERO related to GRB 080207, a photometric redshift has been recently derived (Hunt et al. 2011). The observed broad-band SED implies a very luminous ($M_K \sim 24.4$), infrared-bright galaxy, very different from the sample of GRBHs compiled by SBG09. This host galaxy is similar in color, luminosity, and redshift to the hosts of the dark bursts GRB 080325 (Hashimoto et al. 2010) and GRB 080607 (Chen et al. 2010, 2011). In fact, there may be a possible bias in the GRB host samples studied so far, which are dominated by host galaxies of optically detected afterglows. This conclusion agrees with recent work on dark bursts observed with GROND (Krühler et al. 2011), where it is shown that highly extinguished afterglows trace a subpopulation of luminous, massive, metal-rich, and chemically evolved GRBHs that were not previously associated with GRBs.

5. Summary

Motivated by the non-detection of the optical afterglows of a substantial fraction of *Swift* bursts with well-observed X-ray afterglows, we have selected 17 such events with small *Swift*/XRT error circles (defined by their individual 90% c.l. radius r_0) and searched for the potential host galaxies of these bursts using deep multi-colour imaging. Our primary telescope was the VLT equipped with FORS1, FORS2, & VIMOS for R_C -band imaging and ISAAC & HAWK-I for K_s -band imaging. This was supplemented by observations with the 7-channel imager GROND mounted at the 2.2-m MPG/ESO telescope on La Silla and by the infrared imager NEWFIRM mounted at the 4-m Mayall telescope on Kitt Peak. The limiting magnitudes we achieved are deep, usually $R_{\text{AB}} = 26.5$ and $K_{\text{AB}} = 23.5$ as well as $g'r'i'z'JHK = 25.5, 25, 24.5, 24, 22.5, 21.5, 21$ for GROND. The latter data include late-time imaging as well as data gained

⁶ More precisely, we use figure 10 in Gonzalez-Perez et al. (2009) to calculate chance probability values for our EROs.

in Rapid Response Mode, where we did not find evidence for a fading afterglow.

We find up to six events, $\sim 1/3$ of our sample, where the corresponding GRB host galaxy could be Lyman dropped out in the R_C band. In two cases, we do not see any object inside $2r_0$ down to deep flux limits (GRBs 050922B and 080727A); in one event there is only one galaxy within $1r_0$ and $2r_0$ (GRB 081012); and three bursts have a very red galaxy detected only in the K_s -band (GRB 070429A/object D, GRB 080602/object C, GRB 081105/object C). This three bursts belong to a subsample of seven bursts for which we found extremely red objects (EROs, defined as having $(R - K)_{AB} > 3.5$ mag) as confirmed or likely host galaxy. In particular, all three bursts in our sample that are classified as securely dark according to their observed X-ray flux (following J04 and V09) belong to this group. Even though these are low-number statistics, our findings imply that a non-negligible fraction of optically dim bursts may be located in globally dust-enshrouded galaxies.

While the $(R - K)$ color of galaxies emerged as a powerful criterion to identify host galaxy candidates, we also considered chance-probability constraints based on published number counts of (all types of) galaxies on the sky. In nine bursts the chance probability p to find a galaxy of the given R_C -band magnitude in the corresponding 90% c.l. XRT error circle is $\leq 10\%$ (within 1σ), which makes them good host galaxy candidates. In the remaining cases (about $1/2$ of our sample), galaxies were identified but they are not special in any way, either with respect to their $(R - K)$ colors, their magnitudes, or their p -values. However, for four bursts, we find pairs of possibly interacting galaxies in the XRT error circle, potentially a sign of triggered star-formation.

The connection between star-forming activity and dark bursts is even more intriguing for the seven EROs in our sample. This is the most outstanding result of our study. It points to the existence of a subpopulation of GRBHs, characterized by violent star formation, that is missed by host galaxy surveys of bursts with detected optical afterglows. The putative host of GRB 080207 is the most remarkable example ($(R - K)_{AB} = 4.66 \pm 0.40$ mag; Hunt et al. 2011; Svensson et al. 2011). The possibility that a non-negligible fraction of optically dim bursts traces highly dust-enshrouded and possibly submm-bright galaxies makes these bursts interesting cosmological tools to obtain deeper insight into the optically obscured star formation history of the Universe (Berger et al. 2003; Tanvir et al. 2004).

Acknowledgements. A.R. and S.K. acknowledge support by DFG Kl 766/11-3, 13-2, and 16-1. A.R. acknowledges support from the BLANCEFLOR Boncompagni-Ludovisi, née Bildt foundation. A.R., S.K., and A.N.G. acknowledge support by the Deutscher Akademischer Austausch-Dienst (DAAD; project D/08/15024). P.F. acknowledge support by the MICINN Proyecto Internacional ref. AIB2010DE-00287. S.S. acknowledges support by a Grant of Excellence from the Icelandic Research Fund. L.A.A. and E.G. acknowledge the DAAD RISE program. T.K. acknowledges support by the DFG cluster of excellence 'Origin and Structure of the Universe'. A.N.G. and D.A.K. acknowledge support by DFG grant Kl 766/16-1. E.P. and N.M. acknowledge support under AIT Vigoni program 2008-2009. L.K.H. and E.P. gratefully acknowledge a financial contribution from the agreement ASI-INAF I/009/10/0. F.O.E. acknowledges funding of his Ph.D. through the DAAD. J. Go. and A.J.C.T. are funded by the Spanish research programmes AYA-2007-63677, AYA-2008-03467/ESP and AYA-2009-14000-C03-01. M.N. and P.S. acknowledge support by DFG grant SA 2001/2-1. E. Pian acknowledges support from grant ASI I/088/06/0. A.d.P. acknowledges support by the DNRF. Part of the funding for GROND (both hardware as well as personnel) was generously granted from the Leibniz-Prize to Prof. G. Hasinger (DFG grant HA 1850/28-1). A.R., A.N.G., D.A.K. and A.C.U. are grateful for travel funding support through MPE. This research has made use of the NASA/IPAC Extragalactic Database (NED) which is operated by the Jet Propulsion Laboratory, California Institute of Technology, under contract with the National Aeronautics and Space Administration. A.R. and S.K. thank Johan

Fynbo for a careful reading of the manuscript. This work made use of data supplied by the UK Swift Science Data Centre at the University of Leicester. We thank the ESO staff for performing the VLT service observations. We thank the referee for a very careful reading of the manuscript and very valuable comments, which helped to improve the text substantially.

References

- Amati, L. 2006, MNRAS, 372, 233
- Andreev, M., Kurennya, A., & Pozanenko, A. 2008, GCN Circ., 7333
- Barbier, L., Barthelmy, S., Cummings, J., et al. 2006a, GCN Circ., 5403
- Barbier, L., Barthelmy, S. D., Cummings, J., et al. 2006b, GCN Circ., 5595
- Barthelmy, S. D., Markwardt, C. B., Page, K. L., et al. 2007, GCN Circ., 6355
- Beardmore, A. P., Barthelmy, S. D., Cummings, J. R., et al. 2008a, GCN Circ., 7781
- Beardmore, A. P., Burrows, D. N., & Cummings, J. R. 2008b, GCN Circ., 8522
- Beardmore, A. P. & Cummings, J. 2008, GCN Circ., 8487
- Beardmore, A. P., Evans, P. A., Goad, M. R., & Osborne, J. P. 2008c, GCN Circ., 7782
- Beardmore, A. P., Page, K. L., & Evans, P. A. 2008d, GCN Circ., 7785
- Beardmore, A. P., Page, K. L., Evans, P. A., et al. 2008e, GCN Report, 145, 1
- Berger, E., Hurkett, C., Smale, A., & Cominsky, L. 2003, ApJ, 588, 99
- Berger, E., Fox, D. B., Kulkarni, S. R., Frail, D. A., & Djorgovski, S. G. 2007, ApJ, 660, 504
- Berger, E. & Lopez-Morales, M. 2005, GCN Circ., 3639
- Berger, E., Lopez-Morales, M., & Osip, D. 2005, GCN Circ., 3643
- Berger, E. & Rest, A. 2008, GCN Circ., 8624
- Bissaldi, E. 2008, GCN Circ., 8370
- Bloom, J. S., Kulkarni, S. R., & Djorgovski, S. G. 2002, AJ, 123, 1111
- Blustin, A., Hurkett, C., Smale, A., & Cominsky, L. 2005, GCN Circ., 3638
- Bolzonella, M., Miralles, J.-M., & Pelló, R. 2000, A&A, 363, 476
- Breeveld, A. & Guidorzi, C. 2006, GCN Circ., 5580
- Breeveld, A. & Oates, S. R. 2008, GCN Circ., 8232
- Butler, N. R. 2007, AJ, 133, 1027
- Cannizzo, J., Barbier, L., Barthelmy, S. D., et al. 2007, GCN Circ., 6362
- Castro-Tirado, A. J., Bremer, M., McBreen, S., et al. 2007, A&A, 475, 101
- Castro-Tirado, A. J., Cunniffe, R., de Ugarte Postigo, A., et al. 2006, in Presented at the Society of Photo-Optical Instrumentation Engineers (SPIE) Conference, Vol. 6267, Society of Photo-Optical Instrumentation Engineers (SPIE) Conference Series
- Cenko, S. B. 2006, GCN Circ., 5401
- Cenko, S. B., Kelemen, J., Harrison, F. A., et al. 2009, ApJ, 693, 1484
- Chen, H., Perley, D. A., Wilson, C. D., et al. 2010, ApJ, 723, L218
- Chen, H., Perley, D. A., Wilson, C. D., et al. 2011, ApJ, 727, L53
- Christensen, L., Hjorth, J., & Gorosabel, J. 2004, A&A, 425, 913
- Clemens, C., Filgas, R., Greiner, J., et al. 2008, GCN Circ., 8492
- Cobb, B. E. 2008a, GCN Circ., 7318
- Cobb, B. E. 2008b, GCN Circ., 8248
- Conselice, C. J., Bundy, K., U, V., et al. 2008, MNRAS, 383, 1366
- Covino, S., D'Avanzo, P., Antonelli, L. A., et al. 2008a, GCN Circ., 7322
- Covino, S., D'Avanzo, P., Antonelli, L. A., et al. 2008b, GCN Circ., 8233
- Cucchiara, A. & Fox, D. B. 2008, GCN Circ., 7276
- Cucchiara, A., Levan, A. J., Fox, D. B., et al. 2011, ApJ, 736, 7
- Cucchiara, A. & Racusin, J. 2008, GCN Circ., 7268
- Cucchiara, A. & Ukwatta, T. N. 2008, GCN Circ., 7207
- Cummings, J., Barbier, L., Barthelmy, S., et al. 2005a, GCN Circ., 3637
- Cummings, J., Barbier, L., Barthelmy, S., et al. 2005b, GCN Circ., 4033
- Cummings, J., Barthelmy, S., Gehrels, N., et al. 2008, GCN Circ., 8484
- Curran, P. A., Schady, P., & Cummings, J. 2008, GCN Circ., 8488
- D'Avanzo, P., Antonelli, L. A., Covino, S., et al. 2008, GCN Circ., 7269
- de Ugarte Postigo, A., Castro-Tirado, A. J., Jelinek, M., et al. 2007, GCN Circ., 6361
- de Ugarte Postigo, A. & Malesani, D. 2008, GCN Circ., 8366
- Doherty, M., Bunker, A. J., Ellis, R. S., & McCarthy, P. J. 2005, MNRAS, 361, 525
- Dullighan, A., Ricker, G., Butler, N., & Vanderspek, R. 2004, in American Institute of Physics Conference Series, Vol. 727, Gamma-Ray Bursts: 30 Years of Discovery, ed. E. Fenimore & M. Galassi, 467–470
- Elston, R., Rieke, G. H., & Rieke, M. J. 1988, ApJ, 331, L77
- Evans, I. N., Primini, F. A., Glotfelty, K. J., et al. 2010, ApJS, 189, 37
- Evans, P. A., Beardmore, A. P., Page, K. L., et al. 2009, MNRAS, 397, 1177
- Evans, P. A., Beardmore, A. P., Page, K. L., et al. 2007, A&A, 469, 379
- Evans, P. A., Goad, M. R., Osborne, J. P., & Beardmore, A. P. 2008, GCN Circ., 8391
- Evans, P. A. & Oates, S. R. 2008, GCN Circ., 8231
- Filgas, R., Kruehler, T., Greiner, J., et al. 2008, GCN Circ., 8373
- Fontanot, F. & Monaco, P. 2010, MNRAS, 405, 705

- Fox, D. B., Price, P. A., & Berger, E. 2007, *GCN Circ.*, 6420
- French, J., Jelinek, M., Kubanek, P., & de Ugarte Postigo, A. 2008, *GCN Circ.*, 7316
- Fruchter, A. S., Levan, A. J., Strolger, L., et al. 2006, *Nature*, 441, 463
- Fruchter, A. S., Thorsett, S. E., Metzger, M. R., et al. 1999, *ApJ*, 519, L13
- Fugazza, D., D’Elia, V., D’Avanzo, P., Covino, S., & Tagliaferri, G. 2008, *GCN Circ.*, 7293
- Fynbo, J. P. U., Jakobsson, P., Prochaska, J. X., et al. 2009, *ApJS*, 185, 526
- Gehrels, N., Chincarini, G., Giommi, P., et al. 2004, *ApJ*, 611, 1005
- Gilmore, A. C. 2007, *GCN Circ.*, 6412
- Godet, O., Page, K. L., Osborne, J. P., et al. 2005, *GCN Circ.*, 4031
- Golenetskii, S., Aptekar, R., Mazets, E., et al. 2005, *GCN Circ.*, 3640
- Golenetskii, S., Aptekar, R., Mazets, E., et al. 2008, *GCN Circ.*, 7784
- Gomboc, A., Guidorzi, C., Steele, I. A., et al. 2006, *GCN Circ.*, 4738
- Gonzalez-Perez, V., Baugh, C. M., Lacey, C. G., & Almeida, C. 2009, *MNRAS*, 398, 497
- Gonzalez-Perez, V., Baugh, C. M., Lacey, C. G., & Kim, J.-W. 2011, *MNRAS*, 417, 517
- Gorosabel, J., Christensen, L., Hjorth, J., et al. 2003, *A&A*, 400, 127
- Götz, D., Mereghetti, S., Paizis, A., et al. 2008, *GCN Circ.*, 8614
- Greiner, J., Krühler, T., Fynbo, J. P. U., et al. 2009, *ApJ*, 693, 1610
- Greiner, J., Krühler, T., Klose, S., et al. 2011, *A&A*, 526, A30
- Guidorzi, C., Barthelmy, S. D., Evans, P. A., et al. 2006a, *GCN Circ.*, 5575
- Guidorzi, C., Romano, P., Moretti, A., & Vergani, S. 2006b, *GCN Circ.*, 5577
- Guziy, S., Jelinek, M., Gorosabel, J., et al. 2005, *GCN Circ.*, 4025
- Haislip, J. B., Nysewander, M. C., Reichart, D. E., et al. 2006, *Nature*, 440, 181
- Hashimoto, T., Ohta, K., Aoki, K., et al. 2010, *ApJ*, 719, 378
- Hempel, A., Cristóbal-Hornillos, D., Prieto, M., et al. 2011, *MNRAS*, 414, 2246
- Hogg, D. W., Pahre, M. A., McCarthy, J. K., et al. 1997, *MNRAS*, 288, 404
- Holland, S. & Cucchiara, A. 2006, *GCN Circ.*, 5603
- Holland, S. T. 2006, *GCN Circ.*, 5784
- Holland, S. T., Barthelmy, S. D., Chester, M. M., et al. 2006, *GCN Circ.*, 5776
- Holland, S. T., Sbarufatti, B., Shen, R., et al. 2010, *ApJ*, 717, 223
- Hunt, L. K., Palazzi, E., Rossi, A., et al. 2011, in prep.
- Hurkett, C., Beardmore, A., Godet, O., et al. 2006, *GCN Circ.*, 4736
- Hurkett, C., Page, K., Burrows, D., et al. 2005a, *GCN Circ.*, 3636
- Hurkett, C., Page, K., Kennea, J., et al. 2005b, *GCN Circ.*, 3633
- Immler, S., Baumgartner, W. H., Gehrels, N., et al. 2008, *GCN Circ.*, 8021
- Jakobsson, P., Hjorth, J., Fynbo, J. P. U., et al. 2004, *ApJ*, 617, L21 (J04)
- Kann, D. A., Klose, S., Zhang, B., et al. 2011, *ApJ*, 734, 96
- Kann, D. A., Klose, S., Zhang, B., et al. 2010, *ApJ*, 720, 1513
- Kawai, N., Kosugi, G., Aoki, K., et al. 2006, *Nature*, 440, 184
- Kennea, J. A., Burrows, D. N., Hurkett, C., Page, K., & Gehrels, N. 2005, *GCN Circ.*, 3634
- Kennea, J. A. & Stroh, M. 2008, *GCN Circ.*, 8364
- Khamitov, I., Kose, O., Yakut, K., et al. 2008, *GCN Circ.*, 7270
- Kim, J.-W., Edge, A. C., Wake, D. A., & Stott, J. P. 2011, *MNRAS*, 410, 241
- Klose, S., Eislöffel, J., & Richter, S. 1996, *ApJ*, 470, L93
- Klose, S., Greiner, J., Rau, A., et al. 2004, *AJ*, 128, 1942
- Klotz, A., Boer, M., & Atteia, J. L. 2006, *GCN Circ.*, 5576
- Klotz, A., Boer, M., & Atteia, J. L. 2008, *GCN Circ.*, 7267
- Kong, X., Fang, G., Arimoto, N., & Wang, M. 2009, *ApJ*, 702, 1458
- Kornienko, G., Rumyantsev, V., & Pozanenko, A. 2005, *GCN Circ.*, 4047
- Kouveliotou, C., Meegan, C. A., Fishman, G. J., et al. 1993, *ApJ*, 413, L101
- Krimm, H., Barbier, L., Barthelmy, S., et al. 2006a, *GCN Circ.*, 4757
- Krimm, H. A., Hurkett, C., Pal’shin, V., et al. 2006b, *ApJ*, 648, 1117
- Krühler, T., Greiner, J., Schady, P., et al. 2011, *A&A*, 534, A108
- Krühler, T., Küpcü Yoldaş, A., Greiner, J., et al. 2008, *ApJ*, 685, 376
- Kuin, N. P. M. & Stroh, M. C. 2008, *GCN Circ.*, 8365
- Küpcü Yoldaş, A., Greiner, J., Klose, S., Krühler, T., & Savaglio, S. 2010, *A&A*, 515, L2
- Küpcü Yoldaş, A., Yoldaş, A., Greiner, J., et al. 2008, *GCN Circ.*, 7279
- Landsman, W. B. & Immler, S. 2008, *GCN Circ.*, 8027
- Le Floc’h, E., Duc, P., Mirabel, I. F., et al. 2003, *A&A*, 400, 499
- Levan, A., Fruchter, A., Rhoads, J., et al. 2006, *ApJ*, 647, 471
- Levan, A. J. & Wiersema, K. 2008, *GCN Circ.*, 8048
- Li, W. 2006, *GCN Circ.*, 5400
- Lin, H., Kirshner, R. P., Sheckman, S. A., et al. 1996, *ApJ*, 464, 60
- Lipunov, V., Kornilov, V., Kuvshinov, D., et al. 2006, *GCN Circ.*, 4741
- Luckas, P., Trondal, O., & Schwartz, M. 2005, *GCN Circ.*, 3642
- MacLeod, C., Kirschbrown, J., Haislip, J., et al. 2005, *GCN Circ.*, 3652
- Malesani, D., Jakobsson, P., Levan, A. J., Rol, E., & Fynbo, J. P. U. 2008a, *GCN Circ.*, 8039
- Malesani, D., Quirion, P., Fynbo, J. P. U., & Jakobsson, P. 2008b, *GCN Circ.*, 7783
- Malesani, D., Quirion, P., Fynbo, J. P. U., & Jakobsson, P. 2008c, *GCN Circ.*, 7783
- Mangano, V., Sbarufatti, B., La Parola, V., & Baumgartner, W. H. 2008a, *GCN Circ.*, 8620
- Mangano, V., Sbarufatti, B., & Parola, V. L. 2008b, *GCN Circ.*, 8616
- Marin, V. M., Sabater, J., Castro-Tirado, A. J., et al. 2008, *GCN Circ.*, 7291
- McLean, K., Barthelmy, S. D., Baumgartner, W., et al. 2008, *GCN Circ.*, 8029
- Melandri, A., Gomboc, A., Smith, R. J., & Tanvir, N. 2006, *GCN Circ.*, 5579
- Moin, A., Tingay, S., Phillips, C., et al. 2008, *GCN Circ.*, 8466
- Muehleger, M., Duscha, S., Stefanescu, A., et al. 2006, *GCN Circ.*, 5405
- Norris, J., Barbier, L., Barthelmy, S., et al. 2005, *GCN Circ.*, 4008
- Norris, J., Kuttyrev, A., Ganguly, R., Canterna, R., & Pierce, M. 2006, *GCN Circ.*, 4760
- Oates, S. R., Beardmore, A. P., Cummings, J. R., et al. 2008a, *GCN Circ.*, 8227
- Oates, S. R., Ukwatta, T. N., Evans, P., & Breeveld, A. 2008b, *GCN Report*, 168, 1
- Ovaldsen, J.-E., Jaunsen, A. O., Fynbo, J. P. U., et al. 2007, *ApJ*, 662, 294
- Pandey, S. B., Page, M. J., Ziaepour, H. Z., & Oates, S. R. 2006, *GCN Circ.*, 5402
- Pasquale, M. D., Norris, J., Kennedy, T., Mason, K., & Gehrels, N. 2005, *GCN Circ.*, 4028
- Pérez-Ramírez, D., de Ugarte Postigo, A., Gorosabel, J., et al. 2010, *A&A*, 510, A105+
- Perley, D. A., Cenko, S. B., Bloom, J. S., et al. 2009, *AJ*, 138, 1690
- Perley, D. A., Morgan, A. N., Updike, A., et al. 2011, *AJ*, 141, 36
- Piro, L., Frail, D. A., Gorosabel, J., et al. 2002, *ApJ*, 577, 680
- Price, P. A. 2007, *GCN Circ.*, 6371
- Racusin, J. L., Barthelmy, S. D., Baumgartner, W. H., et al. 2008, *GCN Circ.*, 7264
- Rieke, G. H. & Lebofsky, M. J. 1985, *ApJ*, 288, 618
- Rol, E. & Page, K. L. 2006, *GCN Circ.*, 5406
- Rol, E., van der Horst, A., Wiersema, K., et al. 2007, *ApJ*, 669, 1098
- Rol, E., Wijers, R. A. M. J., Kouveliotou, C., Kaper, L., & Kaneko, Y. 2005, *ApJ*, 624, 868
- Rossi, A., de Ugarte Postigo, A., Ferrero, P., et al. 2008a, *A&A*, 491, L29
- Rossi, A., Greiner, J., Küpcü Yoldaş, A., & Yoldaş, A. 2008b, *GCN Circ.*, 7319
- Rossi, A., Kruehler, T., Greiner, J., et al. 2008c, *GCN Circ.*, 8268
- Rossi, A., Schulze, S., Klose, S., et al. 2011, *A&A*, 529, A142
- Rujopakarn, W., Rykoff, E. S., Schaefer, B. E., Yuan, F., & Yost, S. A. 2006, *GCN Circ.*, 4737
- Rujopakarn, W., Swan, H., & Guver, T. 2008, *GCN Circ.*, 8228
- Rykoff, E. S., Schaefer, B. E., & Swan, H. 2007, *GCN Circ.*, 6356
- Salvaterra, R., Della Valle, M., Campana, S., et al. 2009, *Nature*, 461, 1258
- Sari, R., Piran, T., & Narayan, R. 1998, *ApJ*, 497, L17
- Sato, G., Barbier, L., Barthelmy, S., et al. 2006a, *GCN Circ.*, 4751
- Sato, G., Barbier, L., Barthelmy, S. D., et al. 2006b, *GCN Circ.*, 5578
- Savaglio, S., Glazebrook, K., & Le Borgne, D. 2009, *ApJ*, 691, 182 (SBG09)
- Schady, P., Barthelmy, S. D., Baumgartner, W. H., et al. 2008a, *GCN Circ.*, 7314
- Schady, P. & Cannizzo, J. 2007, *GCN Circ.*, 6364
- Schady, P., Evans, P. A., & Krimm, H. 2008b, *GCN Report*, 117
- Schaefer, B. E., Cline, T. L., Hurley, K. C., & Laros, J. G. 1998, *ApJS*, 118, 353
- Schaefer, B. E., Quimby, R., Yost, S. A., & Rujopakarn, W. 2005, *GCN Circ.*, 4010
- Schlegel, D. J., Finkbeiner, D. P., & Davis, M. 1998, *ApJ*, 500, 525
- Sharapov, D., Ibrahimov, M., Pozanenko, A., & Rumyantsev, V. 2006, *GCN Circ.*, 4927
- Sonoda, E., Maeno, S., Tokunaga, Y., & Yamauchi, M. 2005, *GCN Circ.*, 4009
- Spergel, D. N., Verde, L., Peiris, H. V., et al. 2003, *ApJS*, 148, 175
- Stamatikos, M., Barthelmy, S. D., Burrows, D. N., et al. 2006, *GCN Circ.*, 5590
- Stamatikos, M., Barthelmy, S. D., Cummings, J., et al. 2008, *GCN Circ.*, 7277
- Starling, R. L. C., Page, K. L., & Holland, S. T. 2006, *GCN Circ.*, 5783
- Svensson, K. M., Levan, A. J., Tanvir, N. R., Fruchter, A. S., & Strolger, L. 2010, *MNRAS*, 405, 57
- Svensson, K. M., Tanvir, N. R., Perley, D. A., et al. 2011, *MNRAS*, in press (arXiv:1109.3167)
- Tagliaferri, G., Antonelli, L. A., Chincarini, G., et al. 2005, *A&A*, 443, L1
- Tanvir, N. R., Barnard, V. E., Blain, A. W., et al. 2004, *MNRAS*, 352, 1073
- Tanvir, N. R., Fox, D. B., Levan, A. J., et al. 2009, *Nature*, 461, 1254
- Tody, D. 1993, in *Astronomical Society of the Pacific Conference Series*, Vol. 52, *Astronomical Data Analysis Software and Systems II*, ed. R. J. Hanisch, R. J. V. Brissenden, & J. Barnes, 173
- Torii, K. 2005, *GCN Circ.*, 4024
- Tueller, J., Barbier, L., Barthelmy, S. D., et al. 2006, *GCN Circ.*, 5777
- Ukwatta, T., Barthelmy, S. D., Baumgartner, W., et al. 2008, *GCN Circ.*, 8230
- Updike, A., Clemens, C., & Greiner, J. 2008a, *GCN Circ.*, 8627
- Updike, A. C., Milne, P. A., Williams, G. G., & Hartmann, D. H. 2008b, *GCN Circ.*, 7273
- Urata, Y., Kuwahara, M., Tashiro, M., et al. 2006, *GCN Circ.*, 5204
- van der Horst, A. J., Kouveliotou, C., Gehrels, N., et al. 2009, *ApJ*, 699, 1087 (V09)
- Vergani, S. D., Barthelmy, S. D., Beardmore, A. P., et al. 2007a, *GCN Circ.*, 8620

6411

- Vergani, S. D., Romano, P., Guidorzi, C., et al. 2007b, GCN Report, 56.2
 Vrba, F. J., Hartmann, D. H., & Jennings, M. C. 1995, ApJ, 446, 115
 Vrba, F. J., Luginbuhl, C. B., Jennings, M. C., & Hartmann, D. H. 1999, ApJ, 511, 298
 Vreeswijk, P., Fynbo, J., Milvang-Jensen, B., et al. 2008, GCN Circ., 7327
 Wainwright, C., Berger, E., & Penprase, B. E. 2007, ApJ, 657, 367
 Yoldaş, A. K., Krühler, T., Greiner, J., et al. 2008, in American Institute of Physics Conference Series, Vol. 1000, American Institute of Physics Conference Series, ed. M. Galassi, D. Palmer, & E. Fenimore, 227–231
 Ziaeepour, H. Z., Barthelmy, S. D., Cummings, J. R., et al. 2006, GCN Circ., 5398

Appendix A: Additional notes on individual targets: observations by Swift and other facilities

A.1. GRB 050717

GRB 050717 triggered *Swift*/BAT at 10:30:52 UT (Hurkett et al. 2005b). It was a long burst with a duration of $T_{90}(15 - 350 \text{ keV}) = (86 \pm 2) \text{ s}$ (Cummings et al. 2005a) which was also detected by *Konus-Wind* (Golenetskii et al. 2005). *Swift*/XRT began observing 79 s after the trigger and found a bright, fading X-ray source, while simultaneous *Swift*/UVOT observations started 78 s after the trigger and resulted only in upper limits (Hurkett et al. 2005b; Blustin et al. 2005). Unfortunately, XRT was unable to automatically centroid on the burst, leading to a delay of 2.5 hr in the determination of the X-ray position (error circle radius $6'0$; Kennea et al. 2005; see also Hurkett et al. 2005a). The burst is discussed by Krimm et al. (2006b) in detail, it was very luminous and has one of the highest-ever measured peak energies, with a probable redshift $z > 2.7$. Deep ground-based K -band follow-up observations were performed with the du Pont 100-inch telescope at Las Campanas Observatory with a first run starting 37.7 hr after the burst. No fading NIR source was detected (Berger & Lopez-Morales 2005; Berger et al. 2005). Optical observations with the Tenagra 0.35-m telescope at Perth, Australia, did not find a new source down to the limit of the DSS2 red survey (Luckas et al. 2005). Also, PROMPT-5 at Cerro Tololo Inter-American Observatory in Chile automatically observed the field starting 13 hr after the burst. No fading source was found down to $R_C = 21.7$ and $I_C = 21.5$ (MacLeod et al. 2005).

UVOT obtained an upper limit of $\nu > 19.0$ for any afterglow at 420 s (mid-time) after the onset of the burst (Blustin et al. 2005), corresponding to $\nu > 18.3$ after correction for Galactic extinction. Using the observed constraint on the spectral slope $\beta_{\text{OX}} < 0.40$ at the time of the UVOT observations, this corresponds to an upper limit of $R_{\text{AB}} > 18.2$. In the same way, following Rol et al. (2005), at the time of the optical observation the observed (mean) X-ray flux together with the observed (mean) spectral slope β_X predicts a non-extinguished R_{AB} -band magnitude between 14.5 ± 1.5 and 18.2 ± 1.5 , where the brighter magnitude corresponds to $\nu_c = \nu_{\text{opt}}$ and the fainter magnitude to $\nu_c = \nu_X$ (ν_c is the cooling frequency; Sari et al. 1998). According to the criterion of J04, which uses β_{OX} , the burst is dark, while according to the criterion of V09, which uses β_{OX} and β_X , the burst it is not dark (Table 4).

A.2. GRB 050922B

Swift/BAT detected the burst at 15:02:00 UT. It was an image trigger lasting for 168 seconds (Norris et al. 2005). Cummings et al. (2005b) give $T_{90}(15 - 150 \text{ keV}) = (250 \pm 20) \text{ s}$. Because of the image trigger history, Norris et al. (2005)

speculated that it could be a high-redshift event similar to GRB 050904. *Swift*/XRT started observing 342 s after the trigger, UVOT one second later (Norris et al. 2005). A decaying X-ray afterglow was detected (Godet et al. 2005) but no optical counterpart (Pasquale et al. 2005). Several ground-based small telescopes responded to the trigger but found no afterglow candidate either: ROTSE IIIa (upper limit $CR = 17.3$ at 3 min; Schaefer et al. 2005), the 14-inch Automated Response Telescope at the University of Osaka, Japan (upper limit $CR = 15.1$ at 3 min; Torii 2005), the 0.4-m telescope of Ussuriysk Astrophysical Observatory, Russia (upper limit $CR = 16.0$ at 15 min; Kornienko et al. 2005), and the 30-cm telescope at University of Miyazaki, Japan (upper limit $CR = 16.1$ at 21 min; Sonoda et al. 2005).

The INT 2.5-m telescope at Observatorio del Roque de los Muchachos on La Palma obtained an upper limit on the afterglow of $r' > 22.5$ at 49 ks (mid-time) after the onset of the burst (Guziy et al. 2005), corresponding to $r' > 22.4$ after correction for Galactic extinction. There are no X-ray data for the time between about $t = 10$ ks and 100 ks after the burst, but there are for observations from $t \sim 100$ ks to about 1 Ms. The latter data can be used to extrapolate to the X-ray flux at $t = 49$ ks. The spectral slope is then $\beta_{\text{OX}} < 0.39$, corresponding to an upper limit of about $R_{\text{AB}} > 22.3$. Similarly, the observed X-ray flux together with the observed spectral slope β_X at $t = 49$ ks predicts a non-extinguished R_{AB} -band magnitude between 11.1 ± 2.9 and 14.8 ± 3.0 . Using β_{OX} and β_X , the burst is dark according to the criterion of J04 as well as V09 (Table 4).

A.3. GRB 060211A

Swift/BAT triggered on GRB 060211A at 09:39:11 UT (Hurkett et al. 2006). It was a long burst with a duration of $T_{90}(15-350 \text{ keV}) = 126 \pm 5 \text{ s}$ (Sato et al. 2006a; Krimm et al. 2006a). The spacecraft slewed promptly to the BAT position and *Swift*/XRT found a bright, fading X-ray source, while *Swift*/UVOT started observing 183 seconds after the trigger but did not detect any afterglow candidate (Hurkett et al. 2006). ROTSE IIIa, located at Siding Spring Observatory, Australia, and the Moscow Union 'Optic' MASTER robotic system responded to GRB 060211 immediately. ROTSE's automated response took the first image 147 s after the burst, under twilight conditions, while MASTER started 202 s after the GRB trigger. Only upper limits could be reported (Rujopakarn et al. 2006; Lipunov et al. 2006; see also Urata et al. 2006). Also the 2-m Faulkes Telescope North robotically followed-up GRB 060211 starting 5.4 min after the trigger. No fading optical counterpart down to $R \approx 18.5$ was found (Gomboc et al. 2006). Deep upper limits were also reported by Norris et al. (2006), $J > 19.1$ at 17 hr after the burst, and Sharapov et al. (2006), $R > 22$ at 5.5 hr after the burst.

The 1.5-m telescope of Maidanak Astronomical Observatory obtained for the afterglow an upper limit of $R = 22.0$ at ~ 20 ks (mid-time) after the onset of the burst (Sharapov et al. 2006), corresponding to $R = 21.6$ after correction for Galactic extinction. This corresponds to an upper limit of $R_{\text{AB}} > 21.8$. Among all available upper limits for this burst this observation provides the tightest constraints on the spectral properties of the afterglow from the optical to the X-ray band. According to these data, though, GRB 060211A cannot be classified as a dark burst (Table 4).

A.4. GRB 060805A

The burst triggered *Swift*/BAT on May 8, 2006 at 04:47:49 UT (Ziaeeepour et al. 2006). It had a duration of $T_{90}(15 - 350 \text{ keV}) = 5.4 \pm 0.5 \text{ s}$ (Barbier et al. 2006a). *Swift*/XRT began taking data 93 seconds after the BAT trigger. Ground analysis revealed a faint, uncatalogued X-ray source. *Swift*/UVOT started observing 97 seconds after the trigger but no afterglow candidate was detected in any band (Ziaeeepour et al. 2006; Pandey et al. 2006). Further ground-based observations could only provide upper limits. The robotic 0.76-m Katzman Automatic Imaging Telescope (KAIT) at Lick Observatory started observing the field 119 s after the BAT trigger but no afterglow was found ($V > 16.8$, $I > 16.7$; Li 2006). The automated Palomar 60-inch telescope responded to GRB 060805A and started observing 3 min after the burst trigger. No source down to $R > 19$ was found in the XRT error circle (Cenko 2006). Additional upper limits were obtained by the 1.3-m Skinakas Observatory (University of Crete, Heraklion, Greece): $R > 21.5$ at 14 hr after the burst (Muehleger et al. 2006) and by the 2-m Liverpool Telescope on La Palma: $r' > 22.9$ and $i' > 22.6$ at 0.725 and 0.748 days, respectively, after the burst (Rol & Page 2006).

The 2-m Liverpool Telescope observations correspond to $r' > 22.7$, after correction for Galactic extinction. Using $\beta_{\text{OX}} < 1.00$, this corresponds to an upper limit of $R_{\text{AB}} > 22.7$. Among all available upper limits for this burst this observation provides the tightest constraint on β_{OX} and β_{X} (Table 4). However, these constraints do not qualify GRB 060805A as a dark burst, especially because the X-ray afterglow itself was very subluminal.

A.5. GRB 060919

GRB 060919 triggered *Swift*/BAT at 07:48:38 UT (Guidorzi et al. 2006a). It was a long burst with a duration of $T_{90} = (15 - 350 \text{ keV}) = 9.1 \pm 0.2 \text{ s}$ (Sato et al. 2006b). *Swift*/XRT began taking data 87 seconds after the BAT trigger. Ground analysis revealed a faint X-ray source with an revised error circle of $r = 4''.1$ (Guidorzi et al. 2006a,b). *Swift*/UVOT started observing the field 73 seconds after the burst but did not detect an optical counterpart in any band down to deep flux limits (Breeveld & Guidorzi 2006). The robotic TAROT telescope on La Silla started observing 28 s after the trigger. No optical transient was found down to $R > 15.4$ in the first 60 seconds of observations. An upper limit of $R > 15.8$ could be set for any transient up to 382 s after the trigger (Klotz et al. 2006). The Faulkes Telescope South started observing about 2.8 hours after the event. No optical transient was detected down to a limiting magnitude of $R > 19.5$ (Melandri et al. 2006).

The UVOT upper limit at 918 s corresponds to $\nu > 20.0$, after correction for Galactic extinction. Using $\beta_{\text{OX}} < 0.68$, this corresponds to an upper limit of $R_{\text{AB}} > 19.8$. Similar to the previous two bursts, this observation provides the tightest constraints on the spectral properties of the afterglow. Based on these data, GRB 060919 is not a dark burst (Table 4).

A.6. GRB 060923B

Swift/BAT triggered on GRB 060923B at 11:38:06 UT (Stamatikos et al. 2006). It was a single-peaked burst with a duration of $T_{90}(15 - 350 \text{ keV}) = 8.8 \pm 0.1 \text{ s}$ (Barbier et al. 2006b). *Swift*/XRT began observing the field 114 seconds after the BAT trigger and found an uncatalogued X-ray source with a positional accuracy of $2''.8$. *Swift*/UVOT started observing 122 seconds after the burst with the *white* filter but could not detect an afterglow

candidate (Stamatikos et al. 2006; Holland & Cucchiara 2006). No further ground-based follow-up observations were reported in the literature.

UVOT obtained an afterglow upper limit of $\nu > 18.1$ at 295 s (mid-time) after the burst (Holland & Cucchiara 2006), corresponding to $\nu > 18.0$ after correction for Galactic extinction. Using $\beta_{\text{OX}} < 0.62$, this corresponds to an upper limit of $R_{\text{AB}} > 17.9$. Among all available upper limits for this burst this observation provides the tightest constraint on β_{OX} and β_{X} (Table 4). These constraints do not classify GRB 060923B as a dark event.

A.7. GRB 061102

GRB 061102 triggered *Swift*/BAT at 01:00:31 UT (Holland et al. 2006). It was a long burst with a duration of $T_{90}(15 - 350 \text{ keV}) = 17.6 \pm 1 \text{ s}$ (Tueller et al. 2006). *Swift*/XRT began observing the field 100 seconds after the BAT trigger and found an uncatalogued, fading X-ray source (Holland et al. 2006; Starling et al. 2006). *Swift*/UVOT started observing 110 seconds after the trigger with the *white* filter but no afterglow candidate was seen down to a 3σ upper limit of *white* < 18.5 (Holland et al. 2006). Continued observations provided only upper limits in all UVOT bands (Holland 2006). No further ground-based follow-up observations of this event are reported in the literature.

UVOT obtained an even deeper upper limit of $\nu > 20.5$ at 1480 s (mid-time) after the onset of the burst (Holland 2006), corresponding to $\nu > 20.4$ after correction for Galactic extinction. Using the observed $\beta_{\text{OX}} < 1.10$, this corresponds to an upper limit of $R_{\text{AB}} > 20.1$. Among all available upper limits this observation provides the tightest constraints on the afterglow SED, which do not classify GRB 061102 as a dark burst (Table 4).

A.8. GRB 070429A

The burst 070429A triggered *Swift*/BAT at 01:35:10 UT (Barthelmy et al. 2007). It was a long burst with $T_{90}(15 - 350 \text{ keV}) = 163 \pm 5 \text{ s}$ (Cannizzo et al. 2007). *Swift*/XRT started observing 153 s after the trigger and found a fading, uncatalogued X-ray source, while *Swift*/UVOT started observing 211 seconds after the trigger but did not detect an optical counterpart in any band (Schady & Cannizzo 2007). ROTSE-IIIc, located at Mt. Gamsberg, Namibia, started observing 97 s after the burst. No afterglow candidate was found down to $CR > 17.3$ (unfiltered images) for images taken within 3 min after the trigger and down to $CR > 18.0$ within 8 min (Rykoff et al. 2007). Additional data were obtained with the 0.6-m BOOTES-IR/T60 robotic telescope (Castro-Tirado et al. 2006), starting 3.25 hr after the burst but no afterglow was found (de Ugarte Postigo et al. 2007). Deep *K*-band observations with the 4.2-m William Herschel Telescope on La Palma, beginning 4.1 hr after the burst, detected a faint source in the XRT error circle, but no fading behavior was found (de Ugarte Postigo et al. 2007). Within its astrometric errors this source corresponds to object C detected in our observations (see Table 2).

The Gemini North telescope mounted with the GMOS camera observed the field in i' and z' 44 ks (mid-time) after the burst. No afterglow candidate was found (Price 2007). Unfortunately, no magnitude limits were reported. Therefore, we used a conservative upper limit of $R > 24.0$ based on the original Gemini data available in the Gemini archive⁷. This corresponds to an upper

⁷ <http://cadwww.dao.nrc.ca/gsa/>

limit of $R_{AB} > 23.8$. Together with the measured X-ray flux at the same time this leads to $\beta_{OX} < 0.42$ and $\beta_X - \beta_{OX} - 0.5 > 0.14$. According to J04 as well as V09 the burst is dark. The observed X-ray flux predicts a non-extinguished R_{AB} -band magnitude between 17.2 ± 1.5 and 21.0 ± 1.5 . Since the *Swift*/XRT light curve shows a constant decay with a constant spectral slope during the time when the optical upper limit was obtained, we included GRB 070429A in our golden dark burst sample.

A.9. GRB 070517A

The burst triggered *Swift*/BAT at 11:20:58 UT (Vergani et al. 2007a). T_{90} was 9 ± 1 s (Vergani et al. 2007b). *Swift*/XRT clearly detected an afterglow and could even see evidence for a break in the X-ray light curve. *Swift*/UVOT could not observe, however, due to a 4 mag bright star in the field of view. Ground-based optical follow-up was only reported by Gilmore (2007) (UL = DSS2 Infrared at 2.7 hr after the burst) and Fox et al. (2007) using Gemini-South about 16 hr after the burst. The latter authors suggested two afterglow candidates in the XRT error circle but no further observations of these sources were reported in the literature. Therefore, we used their faintest detection ($i' > 24.5$) as an upper limit at 57600 s. Using the corresponding $\beta_{OX} < 0.56$, this translates to an upper limit of $R_{AB} > 24.3$, which does not classify GRB 070517 as a dark burst. However, in our late-time follow-up observations with VLT/FORS1 the brighter object reported by Fox et al. (2007) ($r' = 22.1$) is not visible anymore. Thus, we conclude that this was the optical afterglow of GRB 070517A.

A.10. GRB 080207

GRB 080207 triggered *Swift*/BAT at 21:30:21 UT (Racusin et al. 2008), and had a duration of $T_{90} = 340 \pm 20$ s (Stamatikos et al. 2008). XRT started observing the field 124 seconds after the BAT trigger and detected a bright source in WT mode. After ~ 5000 s it continued observing in PC mode, showing a light curve with a constant decay index. UVOT did not find the afterglow in early observations after 140 s in a *white* finding chart and in later deeper observations (> 1.5 hours, Cucchiara & Racusin 2008). Several limiting magnitudes based on ground-based observations have been reported: $R > 14.3$ at 1607 s (0.45 hours) and $R > 19.0$ at 5049 s (1.45 hours) (TAROT at the Calern observatory, Klotz et al. 2008); $J > 16.7$, $H > 15.9$, $K > 13.9$ at 7.8 hr, 7.7 hr and 10.1 hr after the trigger respectively (60-cm REM telescope on La Silla, D'Avanzo et al. 2008); $R > 21.8$ at 0.759 hr (RTT150 on 1.5-m telescope at the TUBITAK National Observatory, Khamitov et al. 2008); $R > 20.8$ at 13.7 hrs (SuperLOTIS telescope on Kitt Peak observatory, Updike et al. 2008b); GMOS camera on the Gemini South telescope, did not detect the afterglow down to $g'r'i'z' = 24.1, 24.5, 24.2, 25.0$ at 9.8 hr (Cucchiara & Fox 2008); $R > 23.5$ at 9.75 hr (MOSCA mounted at NOT on La Palma; Marín et al. 2008); $J > 23.5$, $H > 22.8$, $K > 21.5$ (VLT/SINFONI, Fugazza et al. 2008); $R > 20.3$ at 1.49 hr and $R > 21.0$ at 4.94 hr (Zeiss-600 at Mt. Terskol observatory, Andreev et al. 2008). Also, GROND did not detect the afterglow in any band down to deep flux limits (Table A.1).

The Zeiss-600 telescope upper limit at 1.69 hr corresponds to an upper limit of $R_{AB} > 20.5$. The observed X-ray flux predicts a non-extinguished R_{AB} -band magnitude between 11.3 ± 1.4 and 15.0 ± 1.4 . According to the criterion of V09 as well as J04 GRB 080207 is a dark burst (Table 4). It entered our golden dark burst sample.

A.11. GRB 080218B

GRB 080218B triggered *Swift*/BAT at 23:57:47 UT and had a duration of $T_{90} = 6.2 \pm 1.2$ s (Schady et al. 2008b). *Swift* slewed immediately to the burst and XRT found a bright, uncatalogued X-ray source that could be localized with an uncertainty of $r = 3''.0$. UVOT started observing 551 seconds after the BAT trigger using the *white* filter. No afterglow candidate was found down to a 3σ limiting magnitude of 20.6 (Schady et al. 2008a). Several limiting magnitudes based on ground-based observations were then reported: $CR > 16$, starting 60 s after the trigger (unfiltered, 0.4-m Watcher telescope, South Africa, French et al. 2008; $I > 21$ and $J > 18.7$ at 3.1 hr after the burst (1.3-m SMARTS telescope equipped with ANDICAM at CTIO, Cobb 2008a); $H > 13.7$ at 2 min and $K > 12.6$ at 8 min after the trigger (60-cm REM telescope on La Silla, Covino et al. 2008a); $B > 22.1$, $V > 22.7$, $R > 22.9$, $I > 22.6$ at about 1 hr and $J > 20.6$, $H > 20.1$, $K_s > 19.4$ at about 3 hr after the trigger using VLT/FORS2 and NTT/SOFI (Vreeswijk et al. 2008). Finally, no transient radio source was detected in the XRT error circle 2 weeks after the burst (Australia Telescope Compact Array, ATCA; Moin et al. 2008). Most important, GROND did not detect the afterglow down to deep limits in all seven bands in spite of a rapid response time (Table A.1).

GROND obtained an afterglow upper limit of $r' > 24.7$ at 11520 s (mid-time) after the onset of the burst (Rossi et al. 2008b), corresponding to $r' > 24.3$ after correction for Galactic extinction. Using the observed spectral slope $\beta_{OX} < 0.18$, this corresponds to an upper limit of $R_{AB} > 24.3$. The observed X-ray flux predicts a non-extinguished R -band magnitude between 15.1 ± 1.5 and 18.9 ± 1.5 . The burst is dark according to the criterion of J04 as well as V09. It entered our golden dark burst sample.

A.12. GRB 080602

Swift/BAT triggered on the burst at 01:30:28 UT (Beardmore et al. 2008a). T_{90} was 74 ± 7 seconds (Beardmore et al. 2008e). The burst was also detected by *Konus-Wind*, observations of this satellite allowed the peak energy to be constrained to be larger than 226 keV (Golenetskii et al. 2008). *Swift*/XRT found a bright, uncatalogued X-ray source resulting in a $5''.8$ error circle. Evidence for substantial X-ray absorption in excess of the Galactic value was found. *Swift*/UVOT started observing 123 s after the trigger but no afterglow candidate was detected. The XRT error circle was finally reduced to just $1''.7$ and $1''.8$, respectively (Beardmore et al. 2008c,d). The only optical follow-up observation was reported by Malesani et al. (2008b) about 3.4 hr after the trigger using the NOT telescope on La Palma. No afterglow candidate was found down to $R > 22.3$ (Malesani et al. 2008c).

UVOT obtained an upper limit of $v > 20.3$ at 504 s (mid-time) after the onset of the burst (Beardmore et al. 2008e), corresponding to $v > 20.2$ after correction for Galactic extinction. Using the observed spectral slope of $\beta_{OX} < 0.05$, this corresponds to an upper limit of $R_{AB} > 20.2$. Following Rol et al. (2005), the observed X-ray flux and spectral slope predicts a non-extinguished R_{AB} -band magnitude between 13.0 ± 0.7 and 16.7 ± 0.7 . According to the criterion of J04 as well as V09 the burst is a dark burst (Table 4). However, because the X-ray light curve is rather flat instead of decaying during the time when the optical upper limit was obtained, the burst does not enter our golden dark sample. Unfortunately no X-ray data is available contemporary to the deep NOT observations.

A.13. GRB 080727A

Swift/BAT triggered on the burst at 05:57:39 UT with a duration (T_{90}) of 4.9 ± 1.0 s. About 109 seconds later *Swift*/XRT began observing the field (Immler et al. 2008), unveiling a light curve with constant decay and evolving spectral index (see the XRT repository, Evans et al. 2007, 2009). UVOT started observing at 113 seconds, no afterglow was found (Landsman & Immler 2008). Also UKIRT on Mauna Kea did not detect the afterglow down to $K > 19.8$ at 0.63 hr after the trigger (Levan & Wiersema 2008). FORS1 on ESO/Paranal observed the field at 17.5 hr and did not detect the afterglow down to the very deep upper limit of $R > 26$ (Malesani et al. 2008a).

Using the observed spectral slope $\beta_{\text{OX}} < 0.85$, the UKIRT upper limit corresponds to an upper limit of $R_{\text{AB}} > 22.8$. Following Rol et al. (2005), the observed X-ray flux and spectral slope at the time when the optical upper limit was obtained predicts a non-extinguished R_{AB} -band magnitude between 17.9 ± 2.2 and 21.6 ± 2.2 . According to the criterion of V09, the burst lies at the boundary region between dark and non-dark events ($\Delta_{\text{min}} = -0.05$; Table 4). Unfortunately no X-ray data is available during the time of the deep VLT observations.

A.14. GRB 080915A

GRB 080915A triggered *Swift*/BAT at 00:02:49 UT (Oates et al. 2008a). It was a long burst with a duration of $T_{90} = (15 - 350 \text{ keV}) = 14 \pm 5$ s (Ukwatta et al. 2008). Unfortunately, due to an observing constraint, *Swift* could not slew to the burst during the first hour after the event, therefore XRT and UVOT could start observing only 3.9 ks after the trigger. Starting at this time *Swift*/UVOT did not detect the optical afterglow (Oates et al. 2008b). ROTSE-IIIc, located at Mt. Gamsberg, Namibia, responded to GRB 080915A automatically and took unfiltered images starting 52 s after the GRB trigger (cloudy conditions, full Moon). No afterglow candidate was found in the BAT error circle down to about $CR > 14$ (Rujopakarn et al. 2008). The robotic 60-cm REM telescope on La Silla started observing 2 min after the trigger. No afterglow candidates fainter than the 2MASS limits were seen in J, H, K (Covino et al. 2008b). Beginning 4.9 ks after the trigger *Swift*/XRT and *Swift*/UVOT started observing. XRT found a faint, fading X-ray source with an error circle of $r = 6''.5$ (Evans & Oates 2008). Only upper limits could be reported for the UVOT bands (Breeveld & Oates 2008). Deep ground-based observations with ANDICAM on the SMARTS 1.3-m telescope at CTIO provided only upper limits of $I > 21.9$ and $J > 20.1$ (mid-exposure time of 1.9 hr after the burst; Cobb 2008b).

Deep prompt follow-up observations of the field were performed with GROND to search for the afterglow (Rossi et al. 2008c). They started 4.9 min after the trigger and lasted for 130 minutes. No evidence for a variable source was found when splitting these observations into two data sets (Table A.1). Second-epoch observations were performed with GROND the following night. Again, no afterglow candidate was found. Using the GROND upper limit of $r'_{\text{AB}} > 22.2$ at 6840 s (mid-time; Rossi et al. 2008c), and $\beta_{\text{OX}} < 0.62$ (Table 4), this corresponds to an upper limit of $R_{\text{AB}} > 22.0$. Following Rol et al. (2005), we can use the observed X-ray flux as well as X-ray slope to predict the non-extinguished R_{AB} -band magnitude. However in this case due to the small number statistics we can only give an upper limit of $R_{\text{AB}} < 21$. According to the criterion of V09, the burst is dark (Table 4), but the X-ray light curve is faint and very un-

certain. Therefore, this burst is not included in our golden dark burst sample.

A.15. GRB 081012

Swift/BAT triggered on the burst at 13:10:23 UT. T_{90} (15-350 keV) was 29 ± 4 sec. The burst was also seen by Fermi/GBM, the peak energy was 320 ± 80 keV (Bissaldi 2008). The XRT began observing the field 49 minutes after the BAT trigger, an X-ray afterglow was found (Kennea & Stroth 2008), the error circle is just $1''.8$ in size (Evans et al. 2008). UVOT started observing 3 min after the XRT; no afterglow candidate was detected (Kuin & Stroth 2008). Deep ground-based follow-up observations were performed using ROTSE IIIa (with the first image 39 s after the burst), the 2.5-m NOT telescope (de Ugarte Postigo & Malesani 2008).

GROND obtained an upper limit on any optical afterglow of $r'_{\text{AB}} > 23.6$ at ~ 70 ks (mid-time) after the onset of the burst (Filgas et al. 2008; Table A.1), corresponding to $r' = 23.5$ after correction for Galactic extinction. Using the observed spectral slope of $\beta_{\text{OX}} < 0.83$, this corresponds to an upper limit of $R_{\text{AB}} > 23.4$. Among all available optical upper limits, this observation provides the tightest constraint on the SED of the afterglow (Table 4). Based on these data the burst is not dark, neither according to J04 nor according to V09.

A.16. GRB 081105

The burst triggered *Konus-Wind*, *Swift*, *AGILE*, *Suzaku* and *INTEGRAL* at 13:26:12 UT. It was localized via IPN only. The burst had a single peak, about 10 seconds long (Cummings et al. 2008). *Swift*/XRT and UVOT started observing the field about 16 hr later. An X-ray afterglow candidate was detected with an original uncertainty of $4''.8$ (Beardmore & Cummings 2008) and later confirmed (Beardmore et al. 2008b). Observations with UVOT could only provide upper limits (Curran et al. 2008).

GROND obtained an afterglow upper limit of $r' > 23.0$ at ~ 46 ks (mid-time) after the burst (Clemens et al. 2008; Table A.1), corresponding to $r' > 22.9$ after correction for Galactic extinction. Using $\beta_{\text{OX}} < 0.61$ this corresponds to an upper limit of $R_{\text{AB}} > 22.8$. This observation provides the tightest constraints on the SED. Based on these data, the burst is not dark (Table 4).

A.17. GRB 081204

The burst was detected by the *INTEGRAL* satellite at 16:44:55 UT. It lasted for about $T_{90} = 20$ s (Götz et al. 2008). *Swift* reacted to the Integral alert, and started observing the field about 2.7 hr after the burst, and found an uncatalogued X-ray source (Mangano et al. 2008a,b). *Swift*/UVOT started observing 3 hr after the trigger in the *white* filter but no source was detected. Berger & Rest (2008) suggested an $r = 23.5 \pm 0.3$ afterglow candidate based on observations with the Magellan/Clay telescope about 9 hr after the trigger.

The field was also observed with GROND which also detect the afterglow candidate observed by Berger & Rest (2008), together with another object, without finding evidence of fading in either source (Updike et al. 2008a). Both objects are discussed in this paper as host candidates (see Sec. 3.3). Stacking the best GROND data, we obtained the revised upper limits reported in Table A.1, centered at a mid-time of 9.6 hr. The GROND upper limit of $r' > 24.1$ corresponds to $r' > 24.0$ after correction for Galactic extinction. Using the observed $\beta_{\text{OX}} < 0.55$ this cor-

responds to an upper limit of $R_{AB} > 23.9$. Following Rol et al. (2005), we can use the observed X-ray flux as well as the X-ray slope to predict the non-extinguished R_{AB} -band magnitude. However in this case due to the small number statistics we can only give an upper limit of $R_{AB} < 23$ in the worse case of a break between optical and X-ray bands. The burst is dark according to V09 (Table 4), but due to the faint XRT light curve and the not well determined high X-ray spectral slope ($\beta_X = 1.93^{+1.56}_{-0.77}$) this burst did not enter our golden dark burst sample.

Table A.1: Summary of the early-time upper limits based on observations with GROND.

#	GRB	t [hr]	Filter	UL
10	080207	9.75	g'	24.0
		9.75	r'	23.6
		9.75	i'	23.1
		9.75	z'	22.3
		9.75	J	21.0
		9.75	H	19.7
		9.75	K_s	19.0
11	080218B	0.75	g'	21.4
		0.75	r'	21.5
		0.75	i'	20.6
		0.75	z'	20.6
		0.75	J	20.8
		0.75	H	18.5
		0.75	K_s	17.8
		3.2	g'	24.6
		3.2	r'	24.7
		3.2	i'	23.9
		3.2	z'	24.7
		3.2	J	22.0
		3.2	H	20.8
		3.2	K_s	20.0
14	080915A	0.15	g'	22.0
		0.15	r'	22.2
		0.15	i'	21.8
		0.15	z'	21.7
		0.15	J	20.1
		0.15	H	18.9
		0.15	K_s	17.6
		0.92	g'	23.0
		0.92	r'	23.5
		0.92	i'	23.0
		0.92	z'	23.1
		0.92	J	21.2
		0.92	H	20.0
		0.92	K_s	18.6
15	081012	19.35	g'	23.2
		19.35	r'	23.5
		19.35	i'	22.8
		19.35	z'	22.8
		19.35	J	21.5
		19.35	H	20.4
		19.35	K_s	19.4
16	081105	12.84	g'	24.0
		12.84	r'	23.0
		12.84	i'	22.1
		12.84	z'	21.8
		12.84	J	20.7
		12.84	H	19.6
		12.84	K_s	18.2
17	081204	9.60	g'	24.2
		9.60	r'	24.1
		9.60	i'	23.2
		9.60	z'	22.4
		9.60	J	20.7
		9.60	H	19.4
		9.60	K_s	18.3

Notes: For early-time observations by other groups see, e.g., the web page of J. Greiner at www.mpe.mpg.de/~jcg/grbgen.html or GRBlog at <http://grblog.org/grblog.php>. In all cases the data given here supersede the values given in the corresponding GRB circulars: GCN 7279, GRB 080207 (Küpcü Yoldaş et al. 2008); GCN 7319, GRB 080218B (Rossi et al. 2008b); GCN 8268, GRB 080915A (Rossi et al. 2008c); GCN 8373, GRB 081012 (Filgas et al. 2008); GCN 8492, GRB 081105 (Clemens et al. 2008); GCN 8627, GRB 081204 (Updike et al. 2008a).

Table A.3: Redshift estimates of the galaxies found in the XRT error circles for different model assumptions on their photometric properties.

#	GRB	Object	(4)	(5)	(6)	(7)	(8)	(9)
1	050717	A	0.5	0.4	1.2	0.9	3.2	1.8
		B	0.7	0.6	1.7	1.2	–	2.4
3	060211	A	0.7	0.6	1.7	1.2	–	2.4
		B	0.4	0.3	0.9	0.7	2.3	1.4
4	060805A	A	0.9	0.7	2.3	1.4	–	3.0
		B	0.5	0.4	1.1	0.8	3.1	1.8
5	060919	A	1.5	1.0	4.2	2.1	–	4.5
6	060923B	A	0.4	0.3	0.9	0.7	2.4	1.5
		C	0.7	0.6	1.7	1.2	–	2.4
		D	1.2	0.9	3.3	1.8	1.5	3.9
7	061102	A	0.6	0.5	1.4	1.0	4.1	2.1
		B	0.5	0.5	1.3	1.0	3.8	2.0
8	070429A	A	0.9	0.7	2.2	1.4	–	2.9
		B	0.6	0.5	1.5	1.0	4.2	2.1
		C	0.6	0.5	1.6	1.1	4.7	2.3
9	070517A	A	1.0	0.8	2.7	1.6	–	3.4
10	080207	A	0.9	0.7	2.4	1.5	–	3.1
		B	1.7	1.1	–	2.4	–	–
11	080218B	A	1.5	1.1	4.4	2.2	–	4.7
		B	0.7	0.6	1.8	1.2	–	2.5
12	080602	A	0.4	0.3	0.8	0.7	2.2	1.4
		B	0.6	0.5	1.4	1.0	3.9	2.0
14	080915A	B	0.2	0.2	0.4	0.4	1.0	0.7
		C	0.8	0.6	1.9	1.3	–	2.6
		D	0.7	0.6	1.8	1.2	–	2.5
		E	1.0	0.8	2.8	1.6	–	3.5
15	081012	A	0.9	0.7	2.4	1.5	–	3.1
16	081105	A	0.5	0.4	1.2	0.9	3.3	1.8
		B	0.6	0.5	1.6	1.1	4.7	2.3
17	081204	A	0.4	0.3	0.9	0.7	2.5	1.5
		B	0.4	0.4	1.1	0.8	2.9	1.7
		C	0.4	0.3	0.9	0.7	2.4	1.5
		D	0.6	0.5	1.5	1.0	4.3	2.2
		E	0.6	0.5	1.6	1.1	4.7	2.3
		F	1.1	0.8	3.1	1.7	–	3.7

Columns (4) to (9) give the redshift of the galaxy for different assumptions on its spectral slope β and absolute magnitude M_R : = (0.0, –18), (1.0, –18), (0.0, –20), (1.0, –20), (0.0, –22), (1.0, –22). In detail see Sect. 4.6. GRB 050922B and GRB 080727A are not included here since they have no host galaxy candidates.

Table A.4: Redshifts estimated via the Amati relation

#	GRB	Data	Model	E_{peak} (keV)	Redshift	σ
2	050922B	BAT	Band	~ 20	$0.1 < z < 3$	3
6	060923B	BAT	CPL	25 ± 7	$z > 0.4$	2
11	080207	BAT	CPL	108 ± 72	$z > 0.9$	2
11	080218B	BAT	CPL	24 ± 15	$z > 0.3$	2
13	080602	KW	CPL	> 226	$z > 1$	2

Notes: BAT stands for *Swift*/BAT, KW for *Konus-Wind*. CPL stands for cut-off power-law.

- ¹ Thüringer Landessternwarte Tautenburg, Sternwarte 5, 07778 Tautenburg, Germany
- ² Instituto de Astrofísica de Canarias (IAC), E–38200 La Laguna, Tenerife, Spain
- ³ Departamento de Astrofísica, Universidad de La Laguna (ULL), E–38205 La Laguna, Tenerife, Spain
- ⁴ Max-Planck-Institut für Extraterrestrische Physik, Giessenbachstraße, 85748 Garching, Germany
- ⁵ University of Rochester, Department of Physics and Astronomy, Rochester, NY 14627-0171, USA
- ⁶ Florida Institute of Technology, Melbourne, FL 32901, USA
- ⁷ Department of Physics and Astronomy, Clemson University, Clemson, SC 29634, USA
- ⁸ Department of Physics and Astronomy, Dickinson College, Carlisle, PA 17013, USA
- ⁹ Universe Cluster, Technische Universität München, Boltzmannstraße 2, 85748, Garching, Germany
- ¹⁰ Dark Cosmology Centre, Niels Bohr Institute, Univ. of Copenhagen, Juliane Maries Vej 30, 2100 København, Denmark
- ¹¹ INAF-IASF Bologna, Area della Ricerca CNR, via Gobetti 101, I–40129 Bologna, Italy
- ¹² Centre for Astrophysics and Cosmology, Science Institute, University of Iceland, Dunhagi 5, 107 Reykjavík, Iceland
- ¹³ American River College, Physics Dpt., 4700 College Oak Drive, Sacramento, CA 95841, USA
- ¹⁴ Instituto de Astrofísica de Andalucía (IAA-CSIC), Glorieta de la Astronomía s/n, 18.008 Granada, Spain
- ¹⁵ INAF-Osservatorio Astrofisico di Arcetri, Largo Fermi 5, I-50125 Firenze, Italy
- ¹⁶ Institute of Astronomy, University of Cambridge, Madingley Road CB3 0HA, Cambridge, UK
- ¹⁷ Università degli Studi di Milano-Bicocca, Piazza della Scienza 2, 20126, Milano, Italy
- ¹⁸ Scuola Normale Superiore di Pisa - Piazza dei Cavalieri, 7 - 56126 Pisa, Italy
- ¹⁹ INAF-Osservatorio Astronomico di Trieste, Via G.B. Tiepolo 11, 34143 Trieste

Table A.2: Log of the late-time optical/NIR observations to search for a GRB host candidate.

#	GRB	Instrument	Filter	Date obs	Calib	FWHM	Exp. (s)
1	050717	GROND	$g'r'i'z'$	2007/07/24-26	SA114-750	1''0	8880
		GROND	JHK_s	2007/07/24-26	2MASS	1''4	7200
2	050922B	FORS2	R_C	2009/08/15	ESO ZP	0''7	2930
		ISAAC	K_s	2009/07/06	2MASS	0''7	1920
		NEWFIRM	K_s	2008/11/08	2MASS	1''2	1800
3	060211A	GROND	$g'r'i'z'$	2007/10/20-22	SA95-190	1''0	10360
		GROND	JHK_s	2007/10/20-22	2MASS	1''6	8400
		NEWFIRM	J	2009/01/17	2MASS	1''1	10200
		NEWFIRM	K_s	2009/01/17	2MASS	1''2	3600
4	060805A	GROND	$g'r'i'z'$	2008/05/05-07	SDSS	0''9	4440
		GROND	JHK_s	2008/05/05-07	2MASS	1''6	3600
5	060919	FORS1	R_C	2008/04/10	SA110-362	0''8	2930
		ISAAC	K_s	2008/05/18	2MASS	0''6	1920
6	060923B	FORS1	R_C	2008/04/05	NGC2437	0''8	2930
		ISAAC	K_s	2008/04/15	2MASS	0''5	1920
7	061102	FORS1	R_C	2008/04/06	NGC2437	0''7	2930
		ISAAC	K_s	2008/04/18	2MASS	0''7	1920
8	070429A	FORS1	R_C	2008/04/08	SA110-362	1''0	2930
		ISAAC	K_s	2008/05/18	2MASS	0''6	2400
9	070517A	FORS1	R_C	2008/04/10	SA110-362	0''6	2930
		ISAAC	K_s	2008/08/05	2MASS	0''5	1920
10	080207	VIMOS	R_C	2010/02/10	PG1047+3	0''8	2930
		ISAAC	K_s	2010/02/07	2MASS	0''6	1920
11	080218B	FORS2	R_C	2009/05/26	PG1047	0''5	2930
		ISAAC	K	2009/03/20	2MASS	0''5	1920
12	080602	GROND	$g'r'i'z'$	2009/11/24	SDSS	1''1	4440
		GROND	JHK_s	2009/11/24	2MASS	1''3	3600
		FORS2	R_C	2009/06/05	NGC7006	0''8	2930
		ISAAC	K_s	2009/07/06	2MASS	0''7	1920
13	080727A	FORS1	R_C	2008/07/27	E5-Stetson	0''8	2930
		ISAAC	K_s	2010/02/10	2MASS	0''6	1920
14	080915A	FORS1	R_C	2008/09/27	E7	1''4	968
		HAWK-I	K_s	2008/09/16	2MASS	0''6	840
15	081012	VIMOS	R_C	2009/10/21	SA98	0''8	2400
		ISAAC	K_s	2009/10/08	2MASS	0''4	1920
16	081105	VIMOS	R_C	2009/10/21	SA98	1''0	2400
		ISAAC	K_s	2009/09/14	2MASS	0''4	1920
17	081204	VIMOS	R_C	2009/10/21	SA98	1''0	2400
		ISAAC	K_s	2009/09/14	2MASS	0''5	1920
		SOFI	J	2010/11/01	2MASS	0''5	3600

Notes for individual targets: GRB 070517A: a candidate optical afterglow was found by Fox et al. (2007) and we identify it as the GRB afterglow based on our data. *Standard star fields:* The fields PG1047+3, E5, E7, NGC 2437, and NGC 7006 are from the internet pages of P. Stetson <http://www3.cadc-ccda.hia-ihp.nrc-cnrc.gc.ca/community/STETSON/>. Landolt equatorial standards stars (SA) for the R_C band were obtained from the internet page of the Canada-France-Hawaii Telescope <http://www.cfht.hawaii.edu/ObsInfo/Standards/Landolt/>. SA standard star fields for GROND optical calibrations are downloaded from the SDSS archive server at <http://www.sdss.org/>. ZP stands for photometric zero point calibration. *Filters:* Observations with FORS2 were performed using the $R_{\text{special}+76}$ filter. FORS1 and VIMOS used the $R_{\text{Bessel}+36}$ filter. The FWHM column refers to the FWHM of the average stellar PSF.

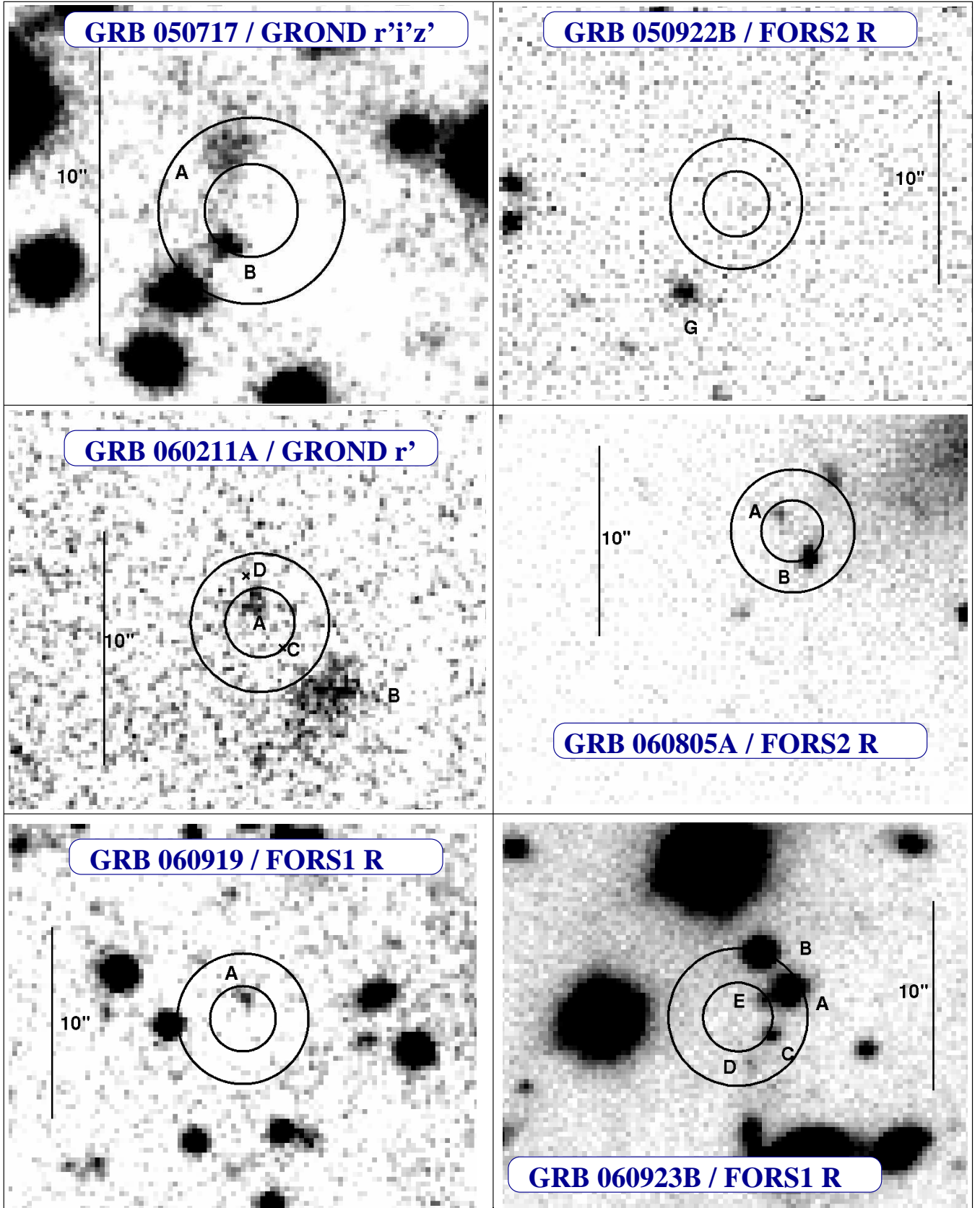


Fig. A.1: The finding charts of our target fields.

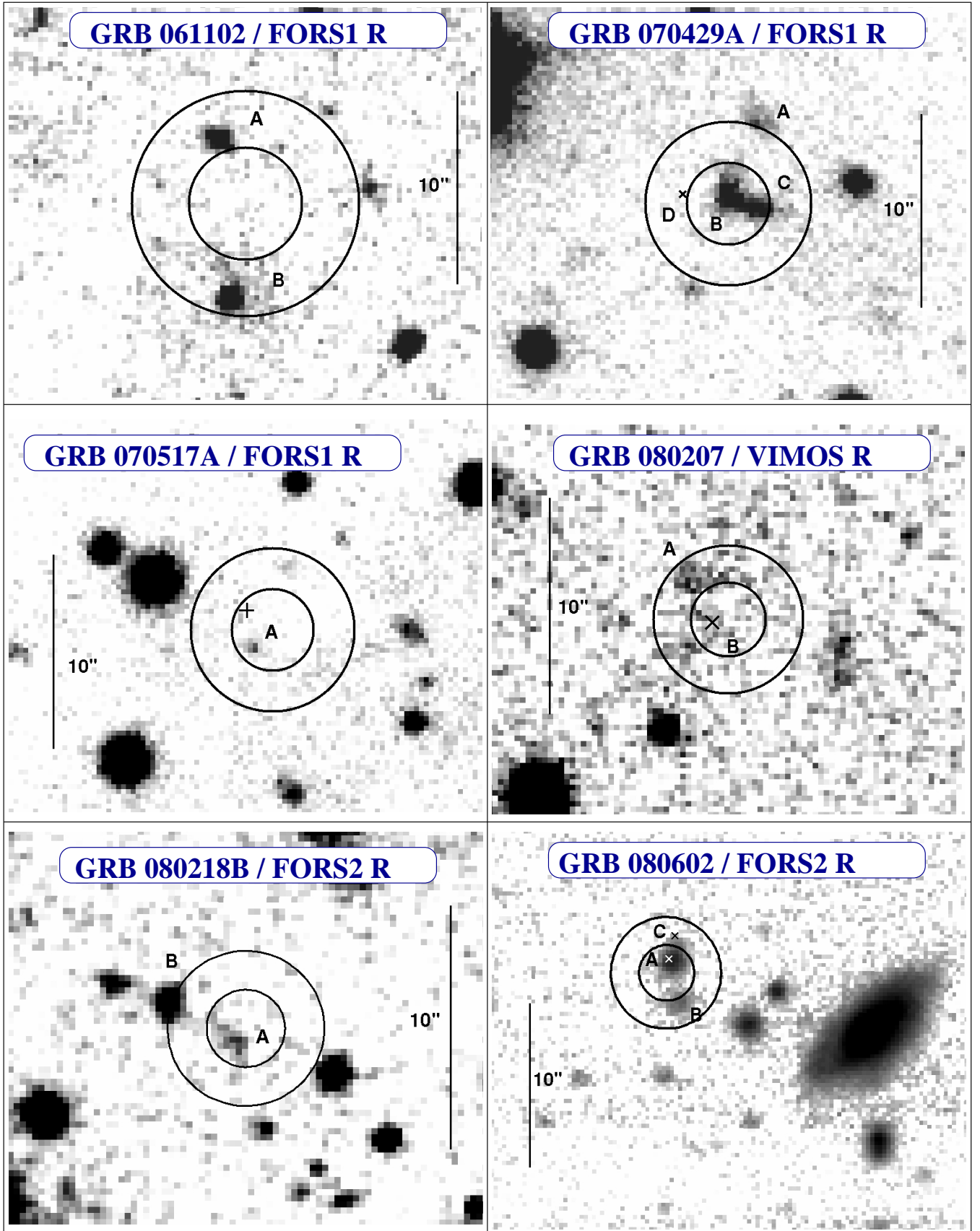


Fig. A.1: continued

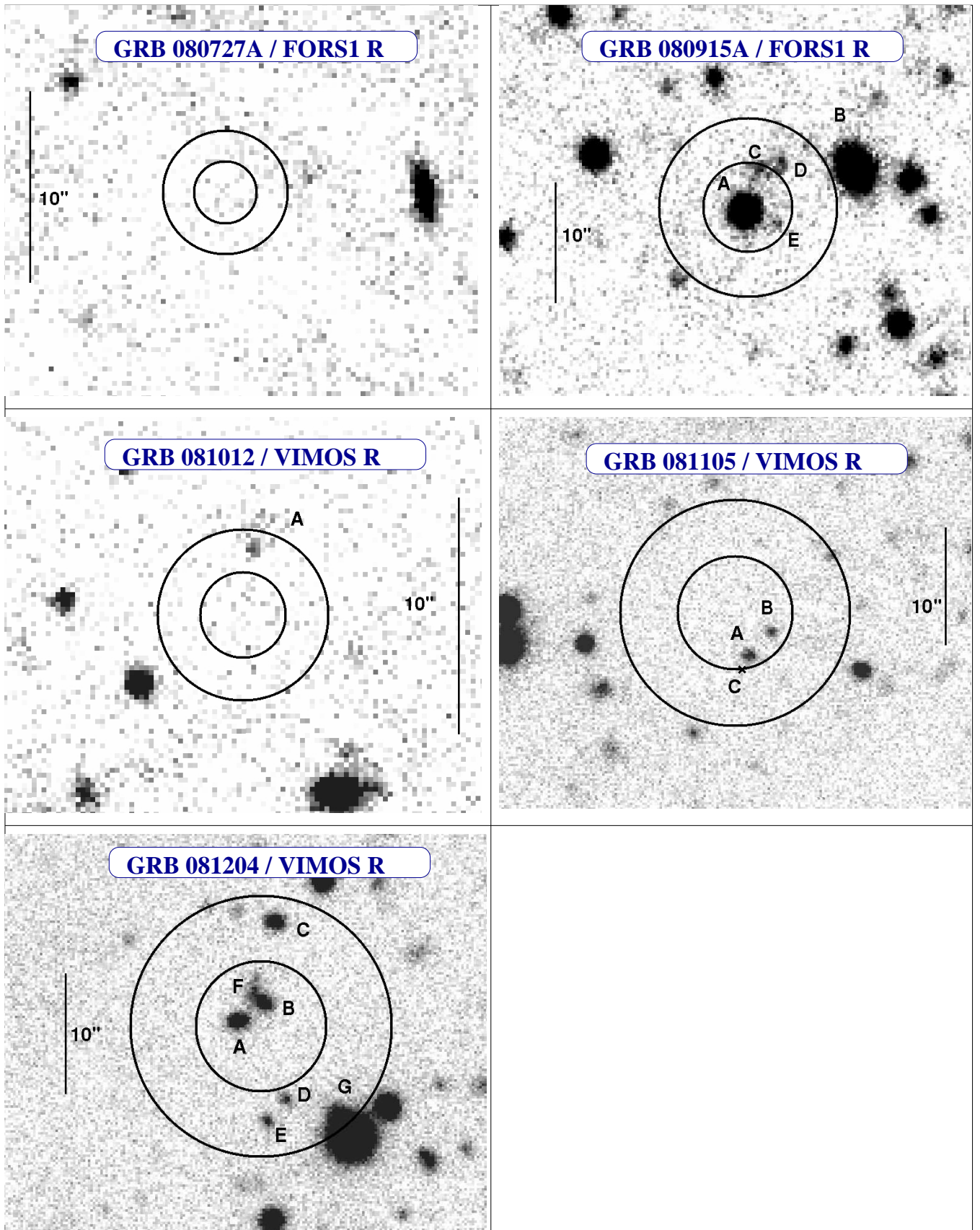


Fig. A.1: continued